UiA University of Agder

Master

Design of an Air Management System for a Dry Room and Utilization of Waste Heat

A Simulink model of an air management system for a dry room used for lithium-ion battery manufacturing has been created. The power demand for temperature control and waste heat temperature of exhaust gasses calculated and the potential for further use of waste heat has been examined.

MORGAN ERIKSEN

SUPERVISOR
Peter Hugh Middleton

University of Agder, 2021
Faculty of Engineering and Science
Department of Engineering Sciences

Abstract

This thesis presents the design of an air management system used in a dry room for a lithium-ion battery factory using a Matlab/Simulink environment. The sizing of the system is based on the 32 GWh battery factory, currently under construction by Morrow Batteries in Arendal, Norway.
The generic air management system from the literature review was used as a base for the general layout and initial values. Combining coolers and a desiccant dehumidification wheel was the optimal solution for the dehumidification system. The molecular sieve was the selected desiccant due to its high performance at low relative humidity. The outlet air quality from the dry room, set to avoid chemical reactions with the battery material, is determined where the moisture content is kept constant at 0.44 gr/lb and a temperature between 22 and 25°C. Baseline simulation for the system uses a structure with the lowest power demand possible whilst maintaining the air quality.
Seasonal fluctuations in ambient conditions bring more moisture into the system with the make-up air, causing an increased power demand and air mass flow in the summer. The sizing of the heat exchanger used in the regeneration loop for the desiccant wheel determines the waste heat temperature. The temperature of the waste heat is 42.64°C as an annual average. The purge rate used in the desiccant wheel is proportional to make-up air and exhaust air, which is a decisive factor for the overall power demand. Further use of this low-grade waste heat depends on local demand and direct use. The use of waste heat for drying wood chips to increase caloric value is a potential solution.

Preface

This thesis is the final step in the Master program in Renewable Energy at the University of Agder in Grimstad, Norway. During the five years, I have gained a broad knowledge about the different renewable energy sources and how to utilize them.

The motivation behind the subject is being part of the evolution of new battery technology due to the growing global demand. To achieve the green shift, development in this area and more efficient management of our energy resources will play a major part. During the writing of this thesis, I have learned a lot about the subject and how to work on a larger project. This has been a valuable learning experience for the future.

I wish to thank my supervisor Peter Hugh Middleton, for guidance and help during this thesis. In addition, thanks to Lars Sigurd Eri, my contact person in Norconsult, who put me on the subject.

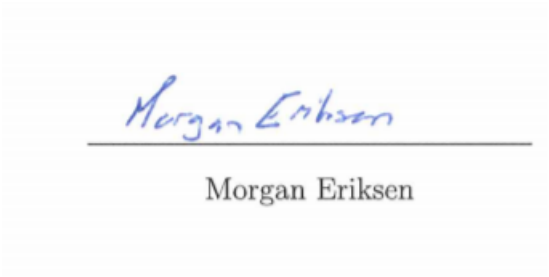

Morgan Eriksen

University of Agder, Grimstad, May 28, 2021

Individual Declaration

1.	I/We hereby declare that my/our report is my/our own work and that I/We have not used any other sources or have received any other help than mentioned in the thesis.	☒
2.	I/we further declare that this thesis: - has not been used for another exam at another department/university/university college in Norway or abroad; - does not refer to the work of others without it being stated; - does not refer to own previous work without it being stated; - have all the references given in the literature list; - is not a copy, duplicate or copy of another's work or manuscript.	☒
3.	I/we am/are aware that violation of the above is regarded as cheating and may result in cancellation of exams and exclusion from universities and colleges in Norway, see Universitets- og høgskoleloven §§4-7 og 4-8 og Forskrift om eksamen §§ 31.	☒
4.	I/we am/are aware that all submitted theses may be checked for plagiarism.	☒
5.	I/we am/are aware that the University of Agder will deal with all cases where there is suspicion of cheating according to the university's guidelines for dealing with cases of cheating.	☒
6.	I/we have incorporated the rules and guidelines in the use of sources and references on the library's web pages.	☒

Publishing Agreement

Authorization for electronic publishing of the thesis.

Author(s) have copyrights of the thesis. This means, among other things, the exclusive right to make the work available to the general public (Åndsverkloven. §2).

All theses that fulfill the criteria will be registered and published in Brage Aura and on UiA's web pages with author's approval.

Theses that are not public or are confidential will not be published.

I hereby give the University of Agder a free right to

make the task available for electronic publishing: ☒JA ☐NEI

Is the thesis confidential? ☐JA ☒NEI

(confidential agreement must be completed and signed by the Head of the Department)

- If yes:

Can the thesis be published when the confidentiality period is over? ☐JA ☐NEI

Is the task except for public disclosure? ☐JA ☐NEI

(contains confidential information. see Offl. §13/Fvl. §13)

Contents

List of Figures

List of Tables

Notations

A	Surface area	[m^2]
a	Lifetime heat exchanger, years	[years]
C	Total cost	[€]
C_{hts}	Total cost for heat exchanger during expected lifetime	[€]
C_p	Specific heat capacity	[kJ/kg K]
G	Moisture load	[kg/s]
$\dot{M}$	Mass flow air	[kg/s]
$\dot{m_w}$	Mass flow waste heat	[kg/s]
Q	Heat transfer rate	[kW]
q	Adsorption heat	[kJ/kg]
S_{hts}	Heat transfer area heat exchanger	[m^2]
ΔT	Temperature difference, T_{out} - T_{in}	[K]
T_a	Ambient temperature	[K]
T_d	Inlet temperature from desiccant wheel	[K]
T_{in}	Inlet temperature	[K]
T_{out}	Outlet temperature	[K]
U	Heat transfer coefficient	[kW/m^2 K]
x	Ratio waste heat to ambient air	[-]
x_a	Humidity ratio inlet air	[-]
x_r	Humidity ratio room	[-]
ω	Moisture content	[kg/kg]

Chapter 1

Introduction

Morrow Battery is a newfound company building a large-scale lithium-ion battery factory at Eyde Energipark, Arendal. The battery factory is yet to be finished but is estimated to be running at full capacity in 2024, with an annual production of 32 GWh distributed to four equal modules. The growing market for electric vehicles (EV's) has lead to the development of new, large battery factories. Norway's advanced process industry and extensive renewable energy supply make it an ideal location for this industry.

The dry room, where the assembly process of the battery cells are conducted, used in these factories requires large amounts of energy for temperature control and dehumidification. This makes it the second largest energy-consuming step, after drying/solvent recovering, with 29.37% of the overall energy demand of the manufacturing process [1]. For this reason, it is interesting to look further into possible ways to make this process more energy-efficient and how different factors affect energy consumption.
The use of renewable energy in power demanding industries will be an essential part of becoming a low-emission society. However, this renewable energy is a limited good and should be utilized to the fullest. Implementing a waste heat recovery system with heat exchangers and a complimentary industry, and creating a synergetic partnership can be a step in the right direction of optimizing energy usage. For battery factories and many others industries, waste heat is released and lost to the surroundings. Even if the the temperature range is low and hard to utilize, it is still wasted energy.

The initiative for the topic of this thesis is from Norconsult, who was interested in the development of the battery factory and looking at the potential for energy saving in the manufacturing process. At the same time, the Norwegian government and the minister of energy proposed a bill where industries with high power demand that are being built or upgraded are required to look into the possibility to utilize waste heat [2]. As the global energy demand keeps rising, it is crucial to find ways to manage our existing energy. According to the minister, focusing on management and efficient use, not only producing more, is the motivation for the initiative. These two reasons, along with a personal interest in developing new and improved battery technology, are the motivation for topic of this thesis.

1.1 Problem Definition

The objective of this thesis is to answer the problems defined below.

- Designing an air management system that can maintain sufficient air quality for a dry room used in lithium-ion battery manufacturing
- Determine how different conditions in the dry room affect power demand and waste heat temperature
- Looking at the potential for further use of the waste heat produced

1.2 Limitations and Assumptions

The study from the literature review has been used for initial values for the air management system. This factory has an annual production of 100,000 lithium-ion batteries for EV's. When the factory is up and running at full capacity, Morrow Batteries will have an annual production of 32 GWh. The battery pack size is currently unknown, but it is possible to make an assumption by comparing the factory to FREYR's factory. This factory is also expected to have an annual production of 32 GWh, producing 600,000 battery packs for automobiles [3], six times that of the literature review. Moisture loads and heat produced in the dry room are expected to follow the size of the factory, making them six times larger as well.

The factory will have four equally sized modules. In this thesis, the results of the power demand, air mass flow and waste heat will take into account the overall results of these four modules combined, looking at the factory as a whole.

The power demand presented will only cover the temperature control for the dry room, mainly for the temperature controlling units. Other factors such as equipment and fans are not taken into consideration.

The prices and cost analysis in this thesis can not be completely validated as they are collected from different sources, where some are estimations. The results are largely based on these prices, but they are meant to work as a guideline showing tendencies with the different solutions and how changes will affect the cost in either direction. If anyone were to use this thesis to recreate a similar system, it is possible to follow the same methodology and change parameters based on the actual values available.

Drying time and consequently the amount of wood chips that could be produced is a bit uncertain. The original temperature range from [4] is not given, only the temperature rise from what is defined as an "ordinary summer day". Average, high temperatures during the three months, June, July and August from Fig. 4.2 is calculated to be 18.2°C, and used as reference point in this thesis.

1.3 Structure of the Report

The structure of the report is as follows. The initial part will cover the relevant theory to support the work conducted in creating the design of the air management system. This includes the operational principles of lithium-ion batteries,dehumidifiers, waste heat recovery, and moist air properties. Following the theory, the literature review is presented, containing the description of a generic air management system. This model is used as a base for the work conducted, with the values functioning as guidelines and initial values.

The next part of the report will describe the dry room conditions, specific for the given factory, and the description of the simulation done using a Matlab/Simulink environment. This includes the sizing of the factory, ambient conditions and other relevant details of the actual Simulink model. Following the simulations, an analysis of the waste heat quality has been conducted, and the potential for further use explored.

In the final part of the report, the results are presented, answering the research question. The discussion reflects on the results, the conclusion sums up the most important points, and a suggestion for further work on the topic is presented.

Chapter 2

Theory

2.1 Lithium-ion Batteries

The lithium-ion battery is the most widespread and used battery for a broad range of applicants. The first commercial use was back in the early 1990's, where small electronic devices started using this new technology [5]. The market for electronics and devices has become gradually saturated. However, as the technology has improved, there is growing potential within transportation, industry and large-scale energy storage [6]. Lithium-ion batteries possess some desirable attributes in higher specific and volumetric energy density than other traditional battery types. These properties result in both lighter and smaller battery compared with other battery types as displayed in Fig. 2.1.

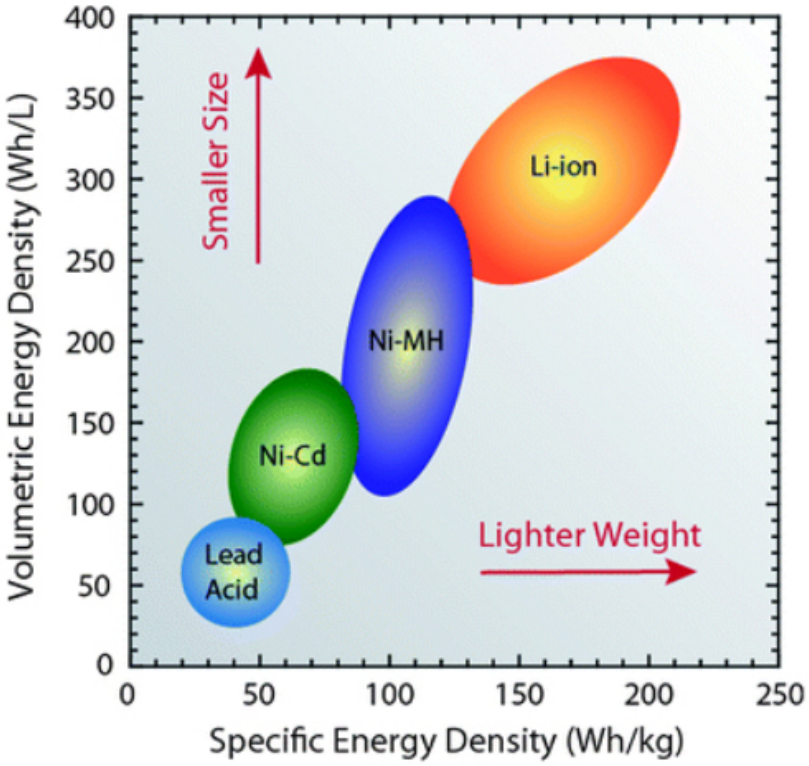

Figure 2.1: Energy comparison of size and weight for different battery types [7]

The batteries cells are manufactured in different forms as displayed in Fig. 2.2, where the main types are cylindrical hard-case, prismatic hard-case or pouch. In terms of production cost, the prismatic pouch has the lowest cost, even if the manufacturing process is more ineffective due to the folding of the cell [8]. However, there are other concerns than only the batteries price in fields such as the automobile industry. Tesla decided to use multiple cylindrical cells in their battery packs instead of larger pouch cells [9]. Using this structure made it possible to install a more efficient cooling system between the cells to improve the performance and lifetime of the cell. A battery management system uses voltage protection during charging to avoid higher capacity cells being charged more than the rest.

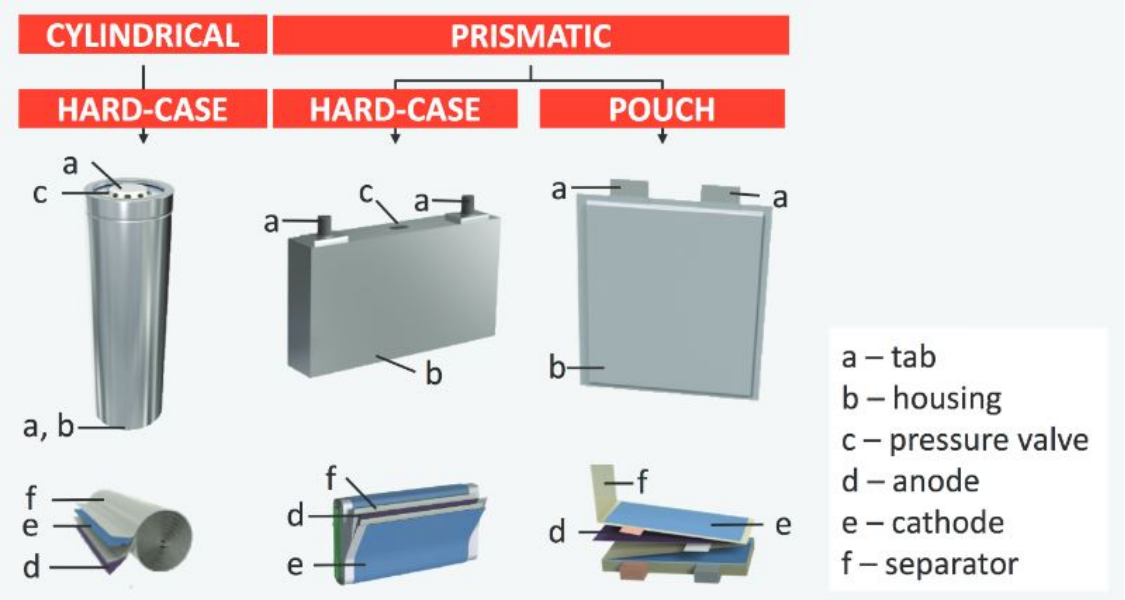

Figure 2.2: Lithium-ion battery cell types [8]

2.1.1 Operating Principles of Lithium-ion Batteries

Fig. 2.3 shows the schematics of a lithium-ion battery cell during discharge and the cell's operating principles. By connecting multiple of these cells, a battery module is created, and these modules connected are called battery packs. Series connection will increase the battery voltage, while the parallel connection gives the battery a higher energy capacity.

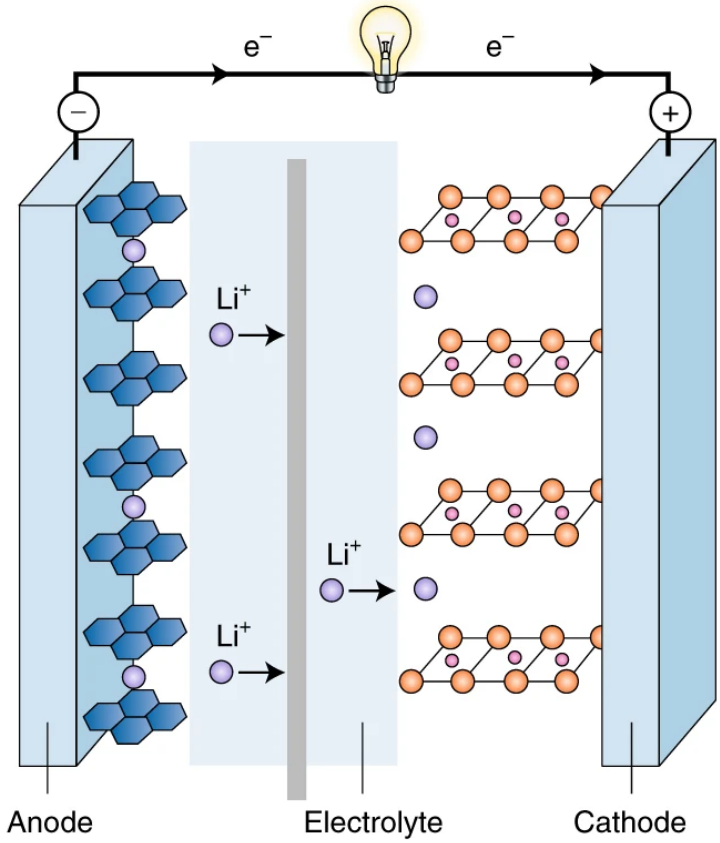

Figure 2.3: Components of a lithium-ion battery cell [10]

The lithium-ion battery consists of a negative and positive electrode, anode and cathode, separated by the electrolyte containing a separator. The cathode side has a metal oxide structure where the lithium is in a stable state. A separated lithium atom is highly reactive and will quickly create a lithium-ion (Li^+) and an electron. The Li^+ will naturally try to return to this stable structure, and by creating a path between it and the metal oxide, electricity can be produced from the electron movement.

The anode has a carbon structure, often graphite, with layers used to trap Li^+. During the charging process of this redox reaction, the active material oxidizes, losing an electron and creating these Li^+ [11]. The electrolyte will only allow the Li^+ through, forcing the electrons through an external circuit. The electrons are drawn to the positive charge from a power supply, separating them from the lithium and creating Li^+. Eqs. (2.1) and (2.2) shows these reactions, using a lithium iron phosphate battery cell as an example.

$$Li\,FePO_4 + Li^+ + e^- \underset{charge}{\overset{discharge}{\rightleftharpoons}} LiFePO_4 \tag{2.1}$$

$$Li \underset{charge}{\overset{discharge}{\rightleftharpoons}} Li^+ + e^- \tag{2.2}$$

After the negatively charged electrons reach the graphite layer, the positively charged lithium-ions are also drawn to the negative terminal and trapped. Once all the lithium-ions are stored at the anode side, the battery is fully charged. The graphite takes no part in the chemical reaction but only works as a storage medium.

This reaction can be reversed by connecting an external load instead of a power supply between the two current collectors. A charged battery is in an unstable state, as the Li^+ wants to move to the metal oxide structure of the cathode. The electron flow through the load creates a current as the electrons return to the cathode. The Li^+ will also move to the cathode but through the electrolyte and not the external circuit. The batteries work according to the electrochemical potential, which can be viewed as a way to measure the difference between the average energy of the outer electron layer of the molecule in its two valence states [12].

2.1.2 Separator

If the battery cell is exposed to large amounts of heat, the electrolyte can dry out, causing a short circuit between the anode and cathode. The separator operates as a built-in fuse to avoid this scenario. By melting at a temperature lower than what is required to dry out the electrolyte, the ion movement is stopped as the pores in the separator are blocked, and the cell shuts down [13]. Without the separator, the drying of electrolyte could cause a fire or explosion, where the cell's temperature will increase rapidly. Fig. 2.4 displays the ideal shutdown of a separator when it reaches its temperatures limit. As the separator with the lowest melting point melts, the pores of the other solids fill, and ion movement stops [14]. This leads to the current drops to 0, while the voltage levels increase to 12V for the given experiment and surface temperature gradually cools down.

The combination of different separator material with different melting points adds to the safety of the battery. Using a combination of polyethylene and polypropylene in a sandwich structure, creating a microporous layer. Ceramic-coated separators can also be used in combination with polyethylene and polypropylene and reduce electrical contact. The separator must be able to withstand physical stress during manufacturing and be both chemically and electronically stable. To avoid unnecessary space and weight, the separator should be as thin as possible while remaining safe and functional. The typical thickness is around 25 μm, but have also been created as thin as 12μm [13][14]. With a thinner separator, the safety concern rises as short circuits can easily happen if metal parts of the battery contact each other. A short circuit can also happen if the battery cells are punctured or in other ways damaged.

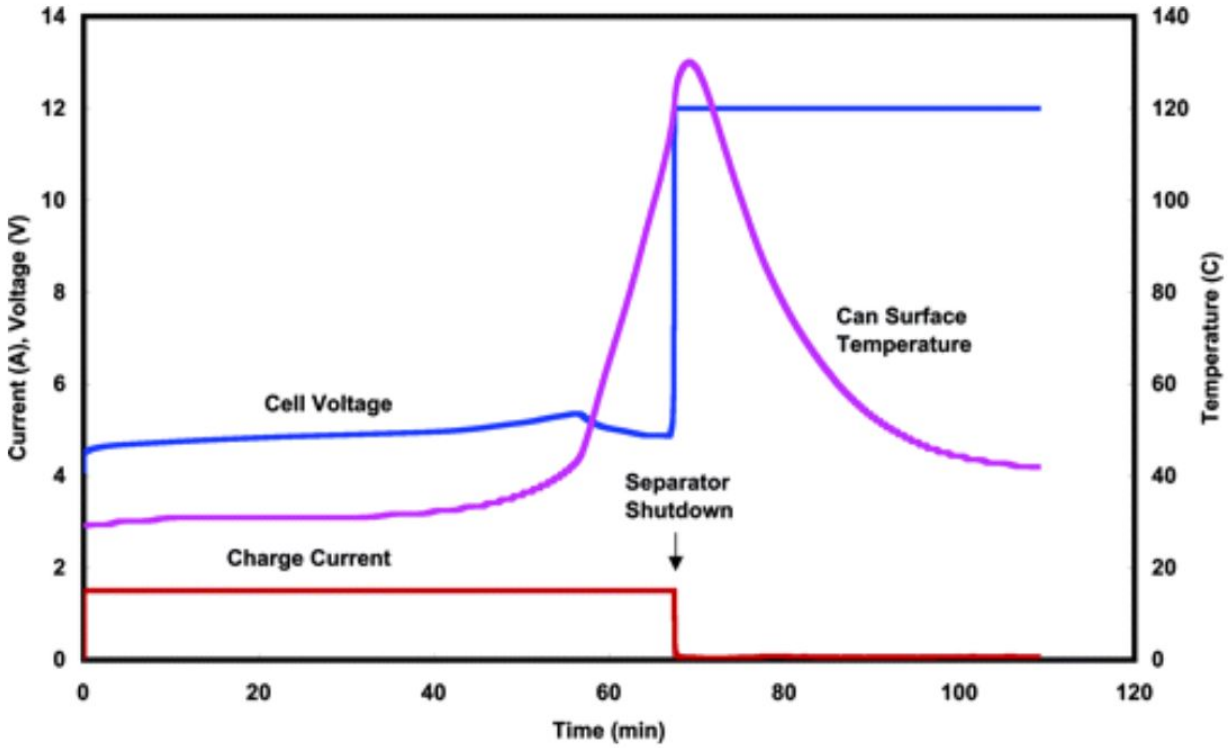

Figure 2.4: Ideal shutdown of a separator used in lithium-ion batteries [14]

2.1.3 Cathode Materials

The energy from transferring electrons determines the chemical potential for the cathode and anode. As different crystal structures are used, the Li^+ flow changes. A higher voltage will carry more energy but will come at the cost of shorter battery life. Using different materials in the lithium-ion batteries makes it possible to get specific characteristics, depending on the battery's application. Table 2.1 shows some of these properties for some of the most common battery types.

Table 2.1: Properties of different cathode materials for lithium-ion batteries [15]

	Li-cobalt	Li-manganese	Li-phosphate	NMC
Voltage [V]	3.6	3.7	3.3	3.6 - 3.7
Charge limit [V]	4.2	4.2	3.6	4.2
Cycle life	500	500 - 1000	1000 - 2000	1000 - 2000
Specific energy [Wh/kg]	150 - 190	100 - 135	90 - 120	140
Specific power [C]	1	10, 40 pulse	35	10
Thermal runaway [°C]	150	250	270	210

Lithium-ion batteries depend on ion movement, which in theory should be able to be everlasting. However, three main factors negatively affect the cycle life; depth of discharge, elevated temperatures and high voltage [16]. Even if the battery reaches the given cycle life, it is not useless but has reached 80% of its original capacity.

The larger the depth of discharge is, the higher the stress at the battery. A full-depth discharge is completely draining and charging the battery, which reduced the battery's capacity faster than partially charging it. Elevated temperature and high voltage will also diminish the battery's capacity, resulting in a shortened cycle life. Even if a high voltage may seem advantageous as it allows for more energy storage, the life cycle is decreased rapidly with a higher voltage [16]. The charge limit determines the desired voltage for the given battery to optimises both performance and longevity.

Specific power in Table 2.1, given in coulomb, describes the battery's load capability. This illustrates the battery's ability for current loading, a desirable attribute for EV's and other high powered applications.

At a given temperature called thermal runaway, the battery cell material will decompose due to an exponential increase in temperature. When this limit is reached, the battery has a self-heating rate higher than the rate it releases to the surroundings and the reaction is out of control. Several different failures can cause this unwanted reaction, either mechanical, thermal failure, short circuit, or electrochemical abuse [17]. With a higher thermal runaway rating, the battery will be safer as it tolerates higher temperatures.

2.1.4 Chemical Reactions with Battery Components

Lithium is a highly reactive metal and will react with both water and air in its pure form. In its pure form, lithium has a metallic shine but as it comes in contact with air, this shine disappears due to reactions with the oxygen and moisture [18]. Eqs. (2.3) and (2.4) show the reactions with oxygen to create lithium oxide and lithium peroxide, while eq. (2.5) shows the reaction with nitrogen to create lithium nitride.

$$4Li_{(s)} + O_{2\,(s)} \longrightarrow 2Li_2O_{(s)} \tag{2.3}$$

$$2Li_{(s)} + O_{2\,(g)} \longrightarrow 2Li_2O_{2\,(s)} \tag{2.4}$$

$$6Li_{(s)} + N_{2\,(g)} \longrightarrow 2LiOH_{(aq)} + H_{2\,(g)} \tag{2.5}$$

Following eq. (2.6), lithium reacts with water, creating the strong base lithium hydroxide and hydrogen gas in an exothermic reaction [18][19]. These reactions can start after the battery has been sealed, potentially causing a fire or explosion when used if the materials are exposed to moisture during manufacturing.

$$2Li_{(s)} + 2H_2O \longrightarrow 2LiOH_{(aq)} + H_{2\,(g)} \tag{2.6}$$

The most commonly used electrolyte in lithium-ion batteries is LiFP6, a lithium salt comprised of an organic solvent. Pure LiFP6 is thermally stable for conditions below 107°C and moisture content of < 10 PPM (parts per million) [20]. The salt is highly reactive to water, following eq. (2.7) the reaction produces lithium fluoride (LiF), phosphoryl oxyfluoride (POF_3) and hydrofluoric acid (HF). Even traces of water will cause this reaction, which causes severe degradation of the battery cells lifetime and performance. HF is an unwanted product of this reaction, as the colourless acid is highly corrosive and can cause damage to both material and personnel.

$$LiPF_6 + H_2O \longrightarrow LiF + POF_3 + 2HF \tag{2.7}$$

Batteries with a high nickel cathode content, such as NMC, are prone to degradation from ambient exposure. Residual lithium on the surface reacts with CO_2, H_2O and O_2 to create Li_2CO_3 and LiOH. An NMC-811 cathode was used in this experiment, which contains 80% nickel, 10% manganese, and 10% cobalt [21]. By exposing the cathode material to ambient conditions for 28 days, the formation of carbonates and oxides created a layer on the surface. The accumulation of these chemicals caused by moisture, carbon dioxide and oxygen increased the charge transfer resistance. The layer created will prevent intercalation, the process where the ions are stored in the metal oxide structure of the cathode, and the performance of the battery cell diminishes.

2.2 Dehumidifiers

The objective of a dehumidifier is to create dry conditions by reducing the moisture content in the air. Dehumidifiers are available in multiple different sizes, from small portable devices to larger industrial applications. There are two main ways of producing dry air; lowering the air temperature to condense the vapour into liquid or using a desiccant to adsorb and remove the moisture from the environment.

The mechanical dehumidifier uses the cooling principle, reducing the temperature of the air below its dew point. Traditionally, mechanical dehumidifiers are used in residential or commercial buildings. They are highly energy-efficient, using electrical power as an energy source.
The desiccant dehumidifiers are more commonly used in industrial applications where very low moisture contents are required. They are not as energy-efficient due to the high temperatures required by the regeneration heater. In comparison to mechanical dehumidifiers, they are more versatile as they can use either thermal energy or electrical power. One of the main advantage of this type of dehumidifier is the ability to lower the air's dew point, rather than freezing the condensed moisture [22]. Desiccant dehumidifiers are divided into either active or passive wheels. The difference is that active wheels use a regeneration heater for the return air to clear the moisture stored in the wheel in a desorption process. Using a combination of both types in a system, the advantages of one will cover the limitations of the other.

The operating principles of an active desiccant dehumidifier wheel are displayed in Fig. 2.5 for a wheel with a 3:1 split between process air and reactivation air inlet areas is used. It is also possible to add a third section called the purge section, which is optional but can reduce power demand and avoid cross-contamination between the two air streams.

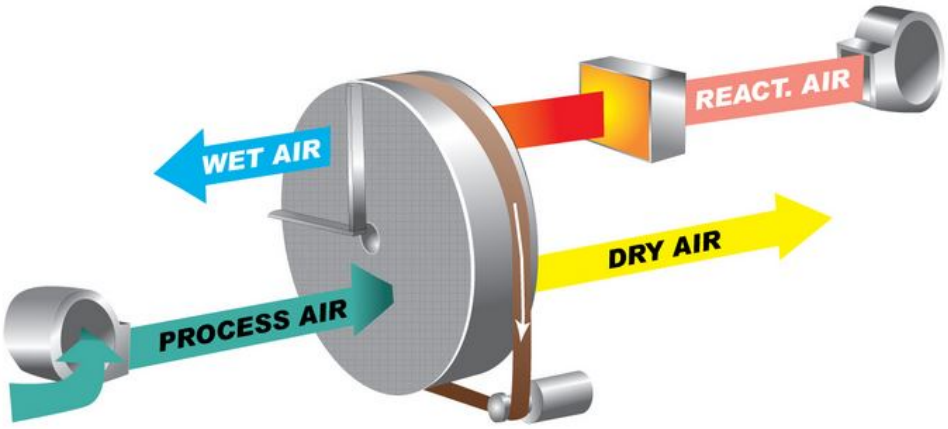

Figure 2.5: Desiccant dehumidifier wheel operating principles [23]

The desiccant dehumidifier wheel operates with two continuous inlet counter airstreams, process and reactivation air. The process air is moist air from a previous stage of the system where the objective is to remove the moisture content from this airflow. The reactivation air is a heated airstream used to clear the wheel for stored moisture, preparing it for the adsorption of new moisture from the process air at the next revolution.

2.2.1 Desiccants

The desiccant wheels consist of a rotor with a honeycomb structure, giving it a large surface covered with a desiccant. The most commonly used desiccants for industrial dehumidification applications are silica gel and molecular sieve. These desiccants, and other commonly used desiccant materials, are displayed in Figs. 2.6 and 2.7 showing the H_2O adsorption capacity and rate.

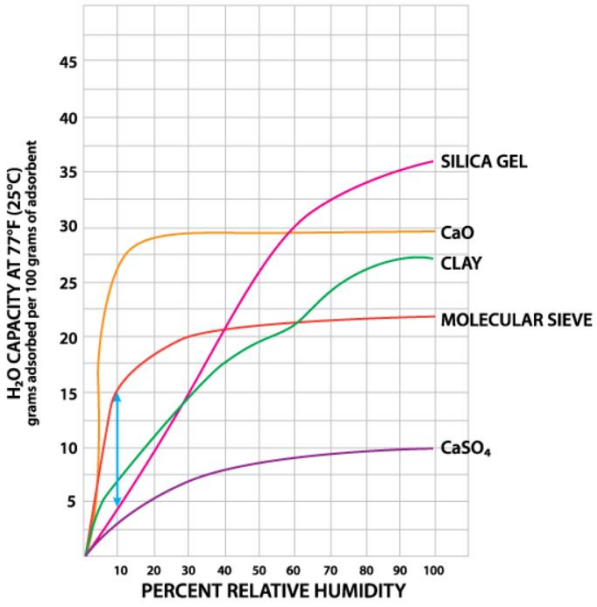

Figure 2.6: H_2O capacity by different desiccants [24]

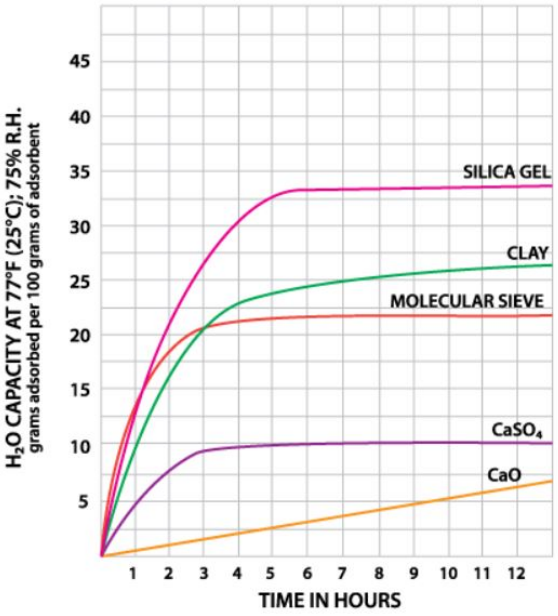

Figure 2.7: Adsorption rate for H_2O by different desiccants [24]

The molecular sieve is a synthetic material containing pores with uniform size and network. The size of the molecular lattice can vary in size from 2-15 Å, a unit of measurement equivalent to 10^{-10} m. The size of the molecular sieve determines the application, as different molecules have different sizes. H_20 is smaller than the CO_2 and O_2, and by using a molecular sieve with 3Å, it will efficiently trap the water molecules while the other gasses get rejected [25][26]. This structure is shown in Fig. 2.8, where the water molecules are adsorbed by the synthetic zeolite materials of the molecular sieve, filling the open pores and gets separated from the air stream.

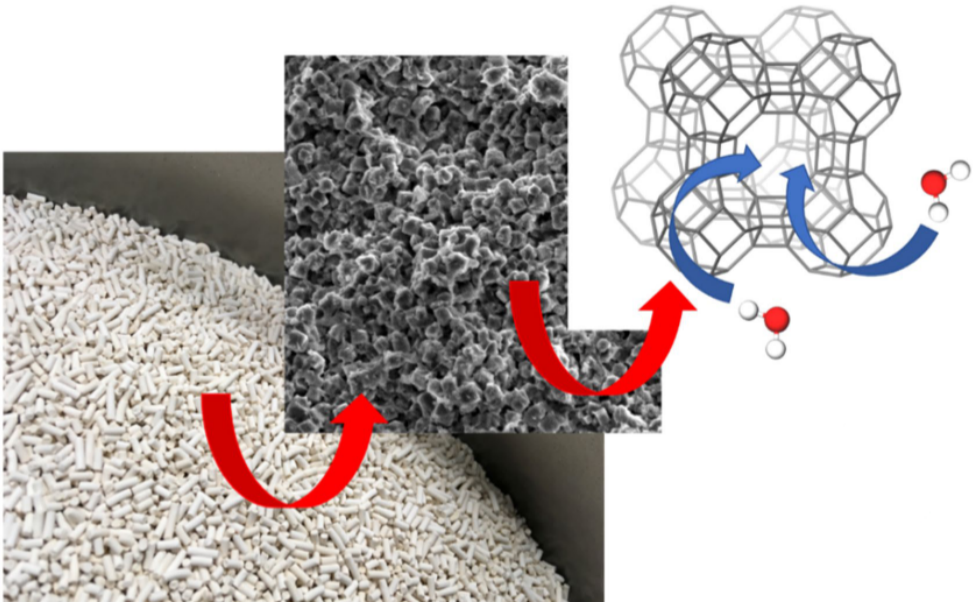

Figure 2.8: Molecular sieve adsorption of H_2O molecules [26]

This water adsorption is an exothermic reaction, as it releases heat to the surroundings equivalent to 4186 kJ/kg (1800 BTU/lb) [24]. The reversed reaction in the desorption process will draw heat from the surroundings in an endothermic reaction, with the same energy as the adsorption of the water. To pass gas through the molecular sieve, it has additional pores and channels. This ensures a free flow through the material and complete utilization of the desiccant. Theoretically, it should be able to store 25% of its weight in moisture, but due to bindings adding up the weight, it is closer to 20%, as displayed in Fig. 2.7. For industrial applications, the adsorption rate is an essential factor to prevent the dehumidification process from becoming a bottleneck or demanding a larger desiccant system. Especially at low relative humidity, the molecular sieve has a high capacity and rate, outperforming the silica gel.

2.3 Waste Heat Recovery

In almost every thermal or mechanical processes, there are some amounts of waste heat produced. Waste heat is excess thermal energy produced as a by-product from another process. Water or air are often used as cooling mediums to maintain the temperature during a process. As the process reaches its practical limit, the waste heat is removed from the area and released. However, there is still energy available in this medium that can be used further by implementing a waste heat recovery system. Waste heat recovery can be divided into two main types; direct or indirect. For direct use, the waste heat remains in its original thermal state and is used by heat pumps, heat exchanger, or for district heating. Indirect waste heat recovery converts the thermal energy to either mechanical or electrical energy by power cycles such as Rankine, Kalina and ORC (Organic Rankine Cycle) or Stirling engines [27].

Different temperatures for waste heat are defined at different ranges depending on the origin and application. In this thesis, the operating range is at the lower end of the spectre, defining high-temperature for temperatures >100°C and low-temperatures <100°C [28]. Higher temperatures are easier to use, as they have a broader range of applications and are more energy dense. Most low-temperature industrial waste heat is currently released into the surroundings as it is hard to utilize it efficiently. Investment costs and low efficient is the reason industries neglect this energy source. Applications for different temperature ranges of waste heat are displayed in Table 2.2. The ranges will be somewhat fluid, but this table gives a general idea of the potential use.

Table 2.2: Applications for waste heat at different temperature ranges [29] [30]

Temperature range [°C]	Application	Example
100 - 120	Drying Power production	Biomass Kalina Cycle
80 - 100	Pasteurization Power production	Dairy ORC
60 - 80	Drying	Bricks, algae
40 - 60	Pasteurization	Beer
20 - 40	Cold air drying Greenhouse Aquaculture Heating	Wood chips Vegetables Fish farming Keeping areas frost free

The first step in waste heat recovery should be to minimize waste heat production in the primary process. Poor heat transfer or overloading heat processing equipment are the main reasons for unnecessary thermal energy is created and lost as waste heat. Once these parts of the system are satisfactory, it is fitting to look at recovery and further use.

2.3.1 Heat Exchanger

A heat exchanger is a device that allows thermal energy to be transferred from one medium, fluid or gas, to another. This process can accrues without any cross-contamination of the two mediums if there are only indirect contact, with a heat transfer area separating them. Heat exchangers can be used in e.g. ventilation systems, vehicles, industrial waste heat from melting, drying or other high-temperature applications [27]. Even if all types of heat exchangers have the same objective, different types are specified for different conditions. The two main types are shell-and-tube, and plate/fin [31]. The shell-and-tube types use a tube containing one of the fluids or gasses while surrounded by the other in the shell, using either parallel, counter or crossflow. The plate/fin heat exchangers have many metal plates, creating a bigger surface area for a faster heat transfer. The rate that the heat can be transferred can be calculated using eq. (2.8), and is a general formula describing heat transfer.

$$Q = \dot{M}\, C_p\, (T_{out} - T_{in}) = U A\, (T_{out} - T_{in}) \tag{2.8}$$

Where:
Q = Heat transfer rate, kW
$\dot{M}$ = Mass flow, kg/s
C_p = Specific heat capacity of medium, kJ/kg K
T_{out} = Temperature out, K
T_{in} = Temperature in, K
U = Heat transfer coefficient, kW/m^2 K
A = Surface area, m^2

In the case of exhaust gasses where heat exchangers are used, deposit corrosive solids can be a problem as it requires either frequent cleaning or advanced materials to withstand corrosion [28]. Heat transfer rate is also often low, as displayed in eq. 2.8, it is a function of temperature differences. With low temperature differences, the heat transfer rate will also be low, and a large surface area is required to collect the energy.

Depending on the origin of the medium, it may contain toxic or unwanted contaminants. Direct and indirect contact condensation recovery offers two different approaches for this problem [28]. For direct condensation, the exhaust gas is mixed with cold water directly, transfers thermal energy, and potentially contaminates the water. By separating the two mediums from each other using a shell and tube heat exchanger, the contamination will be avoided as the heat transfer happens indirectly.

2.3.2 Drying of Biomass

The use of biomass for thermal energy is one of the oldest energy forms used and still relevant today. Calorific value is used as a measurement of the energy available in different types of biomass, given as kWh/m^3 [4]. This value is primarily impacted by the moisture content, which will also reduce the combustion process's efficiency. Therefore, drying biomass is an important step to utilize the energy source to the fullest.

Wood chips originate from various types of biomass divided into smaller parts, which are often used for fuel in heating plants. In its raw form, the moisture content will be $\sim$50% and a calorific value of 504 kWh/m^3. By reducing the moisture content to 20% this values increases to 697 kWh/m^3 due to a more efficient combustion process with less moisture involved [4].

The drying technique called artificial drying uses forced convection by blowing air at the biomass using a fan. With a significantly higher heat transfer coefficient [32], the moisture removal rate increases and drying time reduced. This relationship is displayed in Fig.E.1, where elevated temperatures will contribute to a faster drying process. Solar collectors are used to take advantage of this phenomena, pre-heating the ambient air for biomass drying.

2.3.3 Waste Heat Mediums

The form of the waste heat plays a significant part in the potential range. Industrial waste heat is almost always in one of two forms; gaseous or liquid. Assuming that the properties of the gaseous waste heat are the same as air and that the liquid is water, the different properties are displayed in Table 2.3.

Table 2.3: Comparison between the properties of water and air [33][]

	Heat capacity [kJ/kg K]	Density [kg/m3]	Thermal conductivity [W/m K]
Water	4.184	1,000	0.606
Air	1.005	1.225	0.026

Heat capacity can be defined as the energy required to change a given mass a unit change of temperature. With a higher heat capacity, the material uses more energy to heat up to a higher temperature. However, it will also maintain this temperature for a more extended period, assuming the same conditions as another medium with lower heat capacity. Thermal conductivity describes the ability of a material to conduct heat. This is defined as the quantity of heat transmitted through a given material at a unit thickness to a unit temperature [33]. A higher thermal conductive material will therefore transfer heat at a higher rate. For the two mediums, the largest difference is in the density. In terms of waste heat, this means that it is required a considerable larger amount, in volume, of air to cover the same energy amount for water.

Overall, water is the preferred medium for waste heat applications due to the smaller volume and reduced heat loss in transmission. For both medium, it will be preferable to align the supply of the waste heat with the local demand to create a synergistic relationship between the two parties. Exhaust gasses need to be within proximity of the source, while wastewater can be transported longer distances. The temperature will also play a prominent role in the supply range, where low-grade temperatures have limited distances regardless of the medium.

2.4 Moist Air Properties

The Mollier diagram in Fig. 2.9 is a graphical representation of the interaction between temperature, moisture content, relative humidity and specific enthalpy in moist air. The diagram is a practical way to determine how these factors affect each other when they are changed and knowing the state and properties of the air.

The horizontal lines represent the temperature. Proportionally spaced, they show the temperature of the air given in °C. The vertical lines represent the moisture content of the air, also known as absolute humidity, given as kg/kg. As the diagram displays, the air's capacity to store moisture increases for elevated temperature. The curved lines are for the air's relative humidity. Given as a percentage, where at 100% relative humidity the air has reached its saturation point, and the vapour will start to condense. Specific enthalpy is the final measured property of the air, given as kJ/kg in the diagonal lines. Similarly to the adsorption capacity of moisture, the air's enthalpy is higher for higher temperatures.

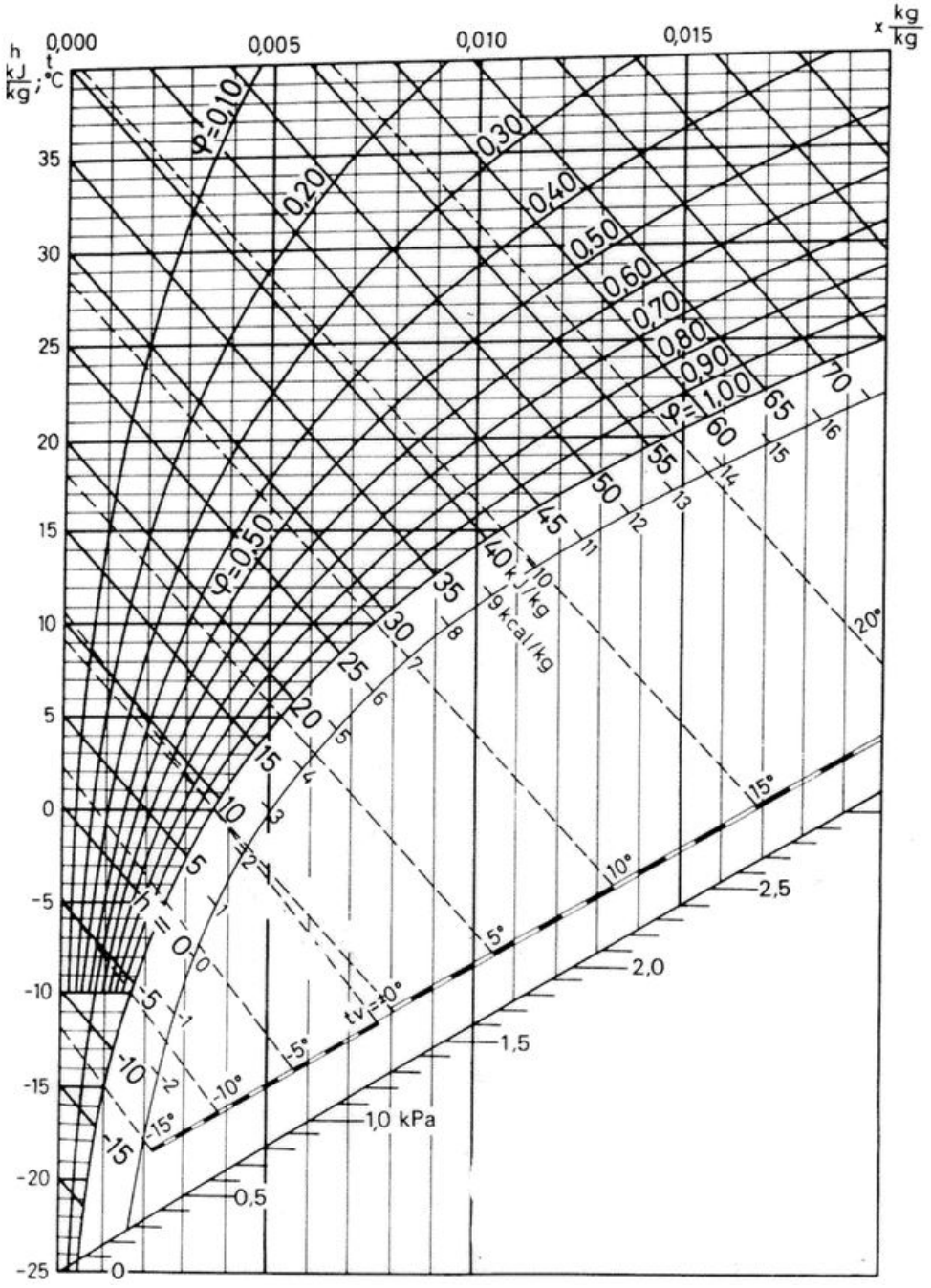

Figure 2.9: Mollier diagram for moist air [34]

Chapter 3

Literature Review

"Study of a Dry Room in a Battery Manufacturing Plant using a Process Model" [35]

This study looks at one of the highest energy-consuming steps in lithium-ion battery production, the dry room. Temperature controlling and drying of large volumes of air is required to maintain sufficient dry room conditions of a moisture concentration of 0.44 gr/lb or 100 parts per million by volume (PPMV) of air.

The generic model created is for a factory assumed to produce 100,000 packs of lithium-ion battery packs for automobiles. The input parameters of the ambient conditions are set at 33°C and relative humidity of 50%. The drying process uses a combination of cooling air and a desiccant dehumidification wheel with molecular sieve to remove the moisture from the air. A regeneration purge air stream of 5% is used to remove contaminants and moisture from the desiccant wheel and the air stream and is included in a loop with a heat exchanger to re-use the thermal energy. There are three primary sources of moisture loads; personnel, negative electrodes, and inlet air.

The study's objective is to determine the price of each battery pack based on the conditions in the dry room air management. Changing the input parameter of the make-up air or structure of the temperature control the overall cost of the production varies. The results presented show the impacts of each of them and give the reader an option for the most important factor for their situation. A decreased purge rate will reduce the energy cost with a resulting lowered make-up airflow rate but increases the possibility of the buildup of contaminants in the desiccant wheel. Similarly, the heat exchanger's sizing has a significant impact on the energy needed for the regeneration heater and adds a new investment and operation cost to the system. By running multiple simulations of these changing parameters, the optimal composition of variable conditions is obtained.

Chapter 4

Dry Room Environment and Simulation of the System

The objective is to create a system of the air management system used in a lithium-ion battery manufacturing dry room. The simulation is used to find the waste heat temperature and determine potential energy saving steps of the manufacturing process, such as purge rate, sizing the heat exchanger for regeneration heat, by using annual ambient conditions. Matlab/Simulink environment is used to create the system and simulate the results. As the battery factory and dry room itself are yet to be built, a generic model is created following similar models, using the available information such as size, the factory's overall capacity, and ambient conditions. Part of finding energy saving steps in the manufacturing process is to look at further use of the waste heat from the factory. The temperature and amount are determining factors and the local requirements at the factory in deciding the best way of utilizing this energy. Temperature control and dehumidification of the air in the dry room is an energy demanding process, especially in humid and hot environments.

The first step of this thesis is to map out the details surrounding Morrow Batteries, including the motivation/reason for the foundation, conditions at the site and required environment inside the dry room. Following the initial gathering of information, the dry room's air management system will be created in Simulink, and the different applications for further use of waste heat are examined.

4.1 Morrow Batteries

The company Morrow Batteries is created by Agder Energi and investor Bjørn Rune Gjelsten to supply the growing demand for batteries used in the transportation sector. The initiative started in 2015 by Frederic Hauge and the environmental foundation Bellona [36], and the factory is expected to be running at full capacity in 2024 [37]. Multiple different locations on the south coast of Norway was considered, and by 12.22.2020, the board of Morrow Batteries unanimously voted Eyde Energipark, Arendal as the factory site [38]. The location is displayed in Fig. 4.1, with the factory to be located north-east of Arendal centre.

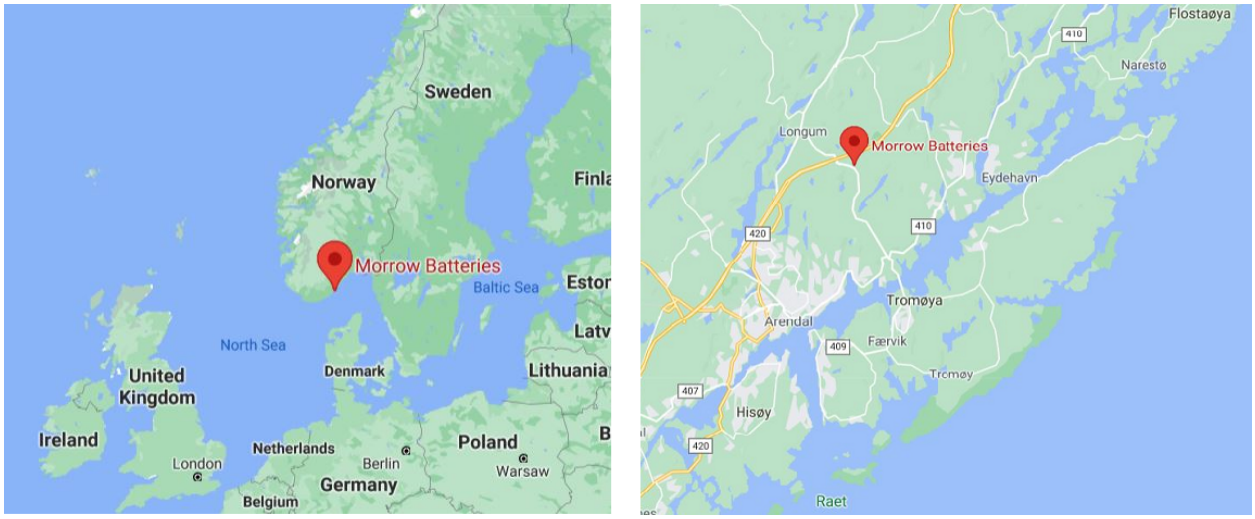

Figure 4.1: Location of Morrow Batteries [39]

According to the company's CEO, Terje Andersen [40], the location close to the European market with connections to airports and a port was critical in selecting the location. This makes it possible to implement Morrow's ambition of sustainability in all production steps to create the greenest battery on the market. By taking advantage of Norway's abundance of clean, renewable energy and advanced process industry, they should compete with the Asian marked [36]. The location is also located between two major areas in the Norwegian industry, Kristiansand and Grenland.

The factory will have a total capacity of 32 GWh, divided into four equal 8 GWh modules [37]. Initially, existing lithium-ion battery technology will be used, but new battery types such as lithium-sulfur are expected to be produced in the future. This part of the market is currently dominated by countries such as China, Japan, and South Korea, where their energy production is mainly coal-fueled. It is estimated that Morrow's factory will have approximately 2,500 workers. For environmental and business reasons, the project has been met with a positive attitude in the local areas. The global battery market is expanding rapidly and will be an important step for the green shift.

The monthly averages of temperatures and humidity for the factory site are displayed in Figs. 4.2 and 4.3. These values will be used at the input signals in the simulation of the system to determine how they affect the energy consumption, waste heat temperatures and air mass flow.

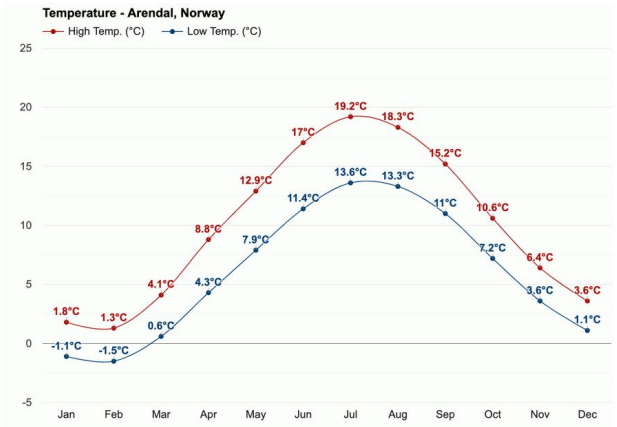

Figure 4.2: Average temperature [41]

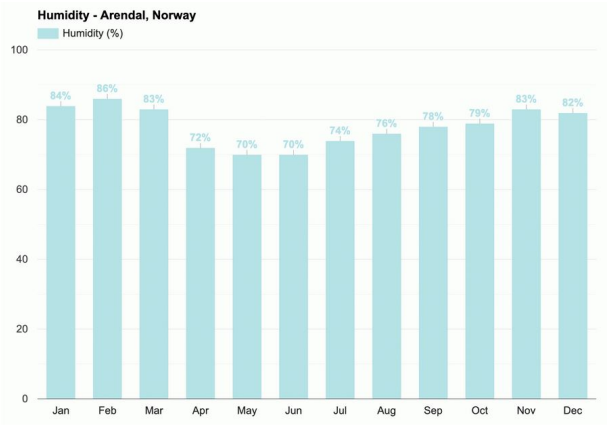

Figure 4.3: Average relative humidity [41]

The temperatures are presented as high and low-temperature averages in °C and the moisture as a relative humidity percentage. These two initial conditions have a significant impact on the energy consumption of the dry room. Elevated temperatures gives the air a higher moisture storing capacity. The relative humidity of the make-up air is the percentage humidity of the total capacity of the given temperature before it reaches saturation.

4.2 Dry Room Environment

To accurately model an air management system for a dry room used in lithium-ion battery manufacturing, it is important to understand how the process of manufacturing the batteries and the specifications of the room. This thesis's dry room is based on the Harris Environmental Dry Room Design [42] and scaled up to the expected size of the 32 GWh in annual production. By following a similar air management system for another dry room described in the literature review, the general layout, temperature, and moisture content limits are used as a starting point. Furthermore, this section aims to obtain the required knowledge of battery production and dry rooms to later on being able to create and simulate an operational air management system.

4.2.1 Lithium-ion Battery Manufacturing

The manufacturing process of lithium-ion batteries are slightly different from factory to factory, but they all follow the same basic principles. This subsection will describe the main steps from raw material to a finished battery, focusing on the cell production and assembly process. This is because the mining and refining of materials are very similar for each factory and do not take place in this given location as the raw materials are imported. The focus of this thesis is the processes accruing during cell production. The manufacturing processes of lithium-ion batteries are divided into three main stages; electrode manufacturing, assembly and electrical formation.

Electrode Manufacturing;
The raw materials used in lithium-ion batteries are mainly graphite, aluminium, lithium and copper. In common for all of them, the raw material has to undergo a mining and refining process before they are delivered to the factory for cell manufacturing. The electrode manufacturing stages are displayed in Fig. 4.4 displays the electrode manufacturing stages.

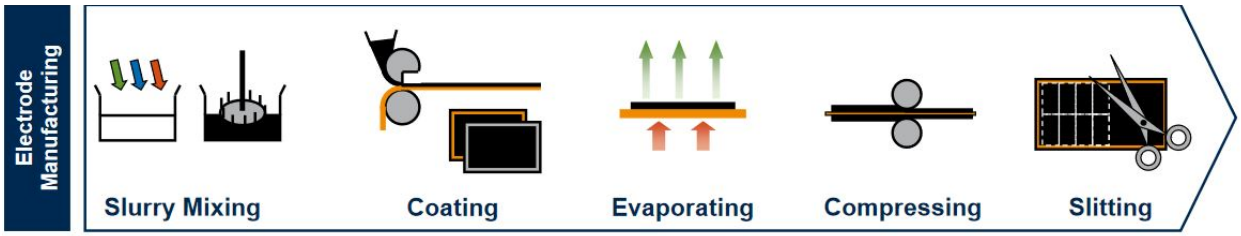

Figure 4.4: Electrode manufacturing stages [43]

The first step of the cell production is mixing this raw material into a slurry by adding NMP-solvent (N-Methyl-2-pyrrolidone), using a rotating container mixer in a vacuum to avoid gas inclusion. This process uses separated mixers for the anode and cathode side of the battery cell. The mixed slurry is used to coat the foil, which creates a thin film on both sides [44][45].
Following the coating process, the film is transported to the first of two drying rooms using a conveyance drying belt to evaporate moisture and solvent from the slurry mixing. Most lithium-ion battery factories have implemented an NMP-solvent recovery system. There is a twofold reason for this, as the solvent is both expensive the toxic. Systems like this are estimated to recover and reuse > 95% [46] of the solvent from the two drying processes by distilling the NMP. This recovery will also make the exhaust gas released from the ventilation system less toxic, making it possible to release into the surroundings as few other hazardous contaminants are released within the factory.
During the compressing process, the foil is compressed using a pair of rotating rollers used to get the thickness of the foil right. The original roll, the mother roll, is divided into smaller rolls called daughter rolls for the final part of the electrode manufacturing process, the slitting.

Assembly;
The first step is the second and final drying process, using a vacuum dryer that removed the residual moisture and solvents at a low temperature. The dried rolls are prepared for the cell assembly by welding the tabs together. A pattern called Z-folding is used for stacking, where continuous layers of anode, separator, cathode, and separator are continuously stacked to a battery cell [44]. The packaging process is slightly different depending on the types of battery cells are manufactured. The current collectors are welded together for the pouched cell, anode to copper and cathode to aluminium. Then the cell is sealed gas-tight on three of four sides, where the fourth is left for the electrode filling. A dosing needle is used to insert the electrolyte into the cell at vacuum conditions

before the pouch cell is sealed. Fig. 4.5 shows the steps in the assembly process.

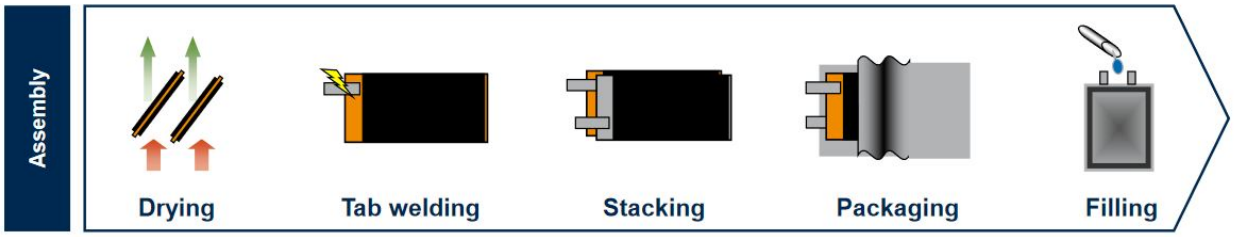

Figure 4.5: Assembly stages [43]

For the prismatic and cylindrical cells, the first step after the stacking is the winding. The prismatic cells use a flat winding, and the cylindrical is winded around a centre pin before they are held together by an adhesive tape. Both cell types are placed in a robust metal housing before the housing and terminals are welded together. Similarly to the pouched cells, the electrolyte filling is done in a vacuum using a dosing needle. With the electrolyte filled, the assembly process is finished.

Electrical Formation;
According to predefined voltage and current curves, the first charge and discharge of the battery cell are called pre-formation. Larger pouch cells are especially prone to the production of gas during the first charging. Therefore the degassing process is implemented where the gas bag is pierced to release the gas, disposed of as hazardous waste. The electrical formation steps are displayed in Fig. 4.6.

Figure 4.6: Electrical formation stages [43]

The cell's ageing is one of the final steps for production, where the cell performance and characteristics are tested during open-circuit voltage. After the final storage period, the battery cell's are ran through an end of line testing to determine the performance and quality before they are packed and shipped away.

4.2.2 Specifications and Conditions

The processes described above are conducted at different locations within the battery factory. The assembly route of the production process in Fig. 4.7 shows the general order followed inside the factory. Different conditions are required for the dry room and the rest of the factory, and for energy-saving reasons, only the assembly process needs dry room conditions. Inside the dry room, there are three main objectives to ensure a sufficient environment;

- Avoid unwanted chemical reactions that can lead to a short circuit of the battery
- Maintain the quality of the product by keeping moisture content and temperature at a constant and set level
- Control the amount of air required in circulation to reduce energy cost for temperature control and dehumidification

The assembly process is the point where the battery materials are most susceptible to small amounts of moisture in the air. At this stage, the material has been dried but are not sealed off from the surroundings yet. Only clean room condition is required to avoid contamination of the cell. Trapping even small traces of moisture inside the sealing would cause unwanted chemical reactions with the material, diminishing the quality and, and in the worst case cause a short circuit. Airlocks surrounding the perimeter of the dry room keeps contaminated air from entering the room.

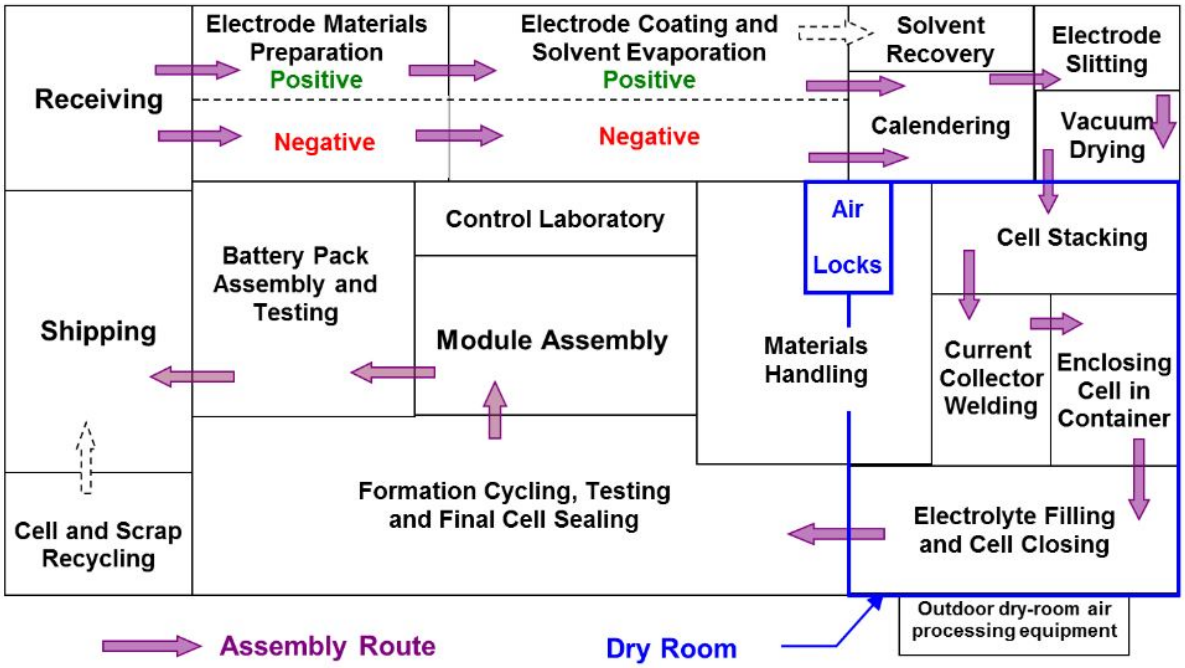

Figure 4.7: Assembly route for lithium-ion battery production [47]

Fig. 4.8 displays the fundamental difference between the clean and dry room. The clean room only requires a filtration system to remove impurities and contamination from the air, while the dry room uses a drying unit to reach very low humidity. A heat exchanger

can also be incorporated to recover heat from the process and reuse it to improve the overall system's energy efficiency. The temperature of the dry room should always be kept within the range of 22-25°C [19][42] and with a dew point between -90°C and -35°C. Heaters and coolers are used to maintain desired temperature ranges throughout the air management system. The dew point can also be viewed as relative humidity or moisture content, and these relationships are displayed in Table B.1.

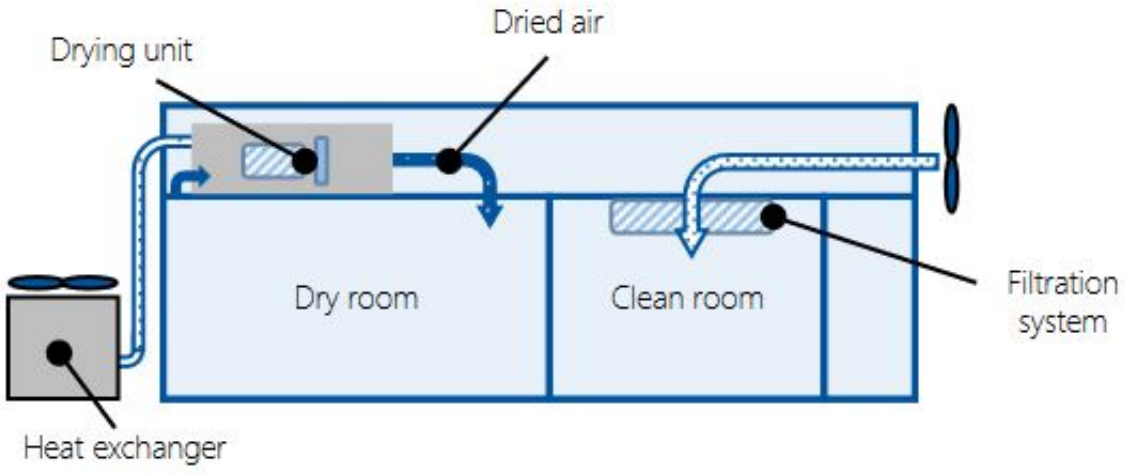

Figure 4.8: Difference between dry rooms and clean rooms [44]

The supply air, dried make-up air, is mixed using an air blender with return air from a previous circulation of the room. The fresh air enters the dry room through vents in the ceiling and enters a pre-cooler before mixing with returning air from the dry room. Moisture transmission through the walls and ceiling is avoided using a vapour tight construction. Metal clad insulated modular panels provides some distinct advantages for dry room constructions. They provide zero vapour transmission from the surroundings, easy to either expand or move the dry room and are simple to install. To ensure that the panels remain vapour proof, either silicon or foam in place urethane is used to cover any joints between modules. The same is the case for ducts or pipes entering and leaving the room. The floor is either covered in sheet vinyl, conductive tiles or using a sealed concrete floor to avoid moisture from the ground transmitting into the room [42].

An airlock prevents the outside moisture and other contamination from entering through the doorways, using pressurized dry air to keep the internal environment at dry room conditions. Dry air from the dehumidification system is used to keep the moisture content in the room low. This dry air absorbs moisture from various moisture loads inside the room to maintain the given moisture content limit. Exhaust air is released to the surroundings, containing moisture and other contaminants from the room, while new make-up air enters the room at the same rate as the exhaust air leaves. The majority of the airflow is reused and mixed with the new air to reduce the cost of temperature control and dehumidification.

4.2.3 Dehumidification System

The objective of the dehumidification system is to dry the air entering the dry room to keep it at dry room conditions. In this system, a desiccant dehumidification wheel is used in combination with coolers. By combining mechanical dehumidification and adsorption with desiccants, the system becomes as energy-efficient as possible whilst providing dry room conditions. This types of system can also incorporate clean, renewable energy sources, making the process potentially emission-free.

There are two main types of desiccant materials used for desiccant wheels: silica gel and molecular sieve. The conditions and applications determines which is the most suitable of the two. For conditions with high moisture content and relative humidity, >40%, the silica gel has a higher H_2O adsorption capacity and is the best choice [48]. This is often the case for residential use, where the moisture content can be higher than for industrial applications. The environment inside the dry room demands low dew point and conditions with very low relative humidity. Due to the pre-cooler and the air blender mixing, the inlet air to the desiccant wheel has an already low moisture content. This makes the molecular sieve the best option for the desiccant wheel used in a dry room for lithium-ion battery manufacturing.

The molecular sieve uses physical adsorption to capture the water molecules. The adsorption of water molecules releases energy when the bonds are created. This exothermic reaction releases what is called adsorption energy, set to be 4186 kJ/kg. Following eq.(4.1), the adsorption heat is calculated, which is the temperature change from either adsorbing or desorbing the water molecules to and from the desiccant. The endothermic desorbtion process draws energy from the surrounding, and is the reversed adsorption process.

$$\Delta T = \omega * \frac{q}{C_p} \tag{4.1}$$

Where:
ΔT = Temperature change, K
ω = Moisture content, kg/kg
q = Adsorption heat, kJ/kg
C_p = Heat capacity air, kJ/kg K

The temperature change depends on the adsorption rate of moisture from the air, which directly correlates to the amount of moisture removed from the air. The desiccant wheel is divided into three main sections for different airflows; process air, regeneration air, and purge section. The most commonly used division between the process air is either 3:1 or 1:1, process air to regeneration air. Using the 3:1 requires a higher regeneration temperature to recover the moisture from the wheel and utilize a larger inlet process airstream for adsorption. The correlation between the sections' size and regeneration temperature makes it possible to use a lower temperature for the 1:1 division.

The third and final section, purge section or purge angle, is optional for the desiccant wheel. This purge angle can be defined as the ratio of moisture removed from the inlet air per unit time to the amount of heat required to regenerate the desiccant wheel per unit time. The optimum angle for a wheel using hot regeneration temperature between 140 and 170°C is 29.7° [49]. Converting to the percentage of the wheel area, this amounts to 8.17%, which will be used for the purge rate of the air stream in the simulations, making the reuse rate the remaining 91.83%. Fig. 4.9 shows the different sections and the wheel itself from different angles.

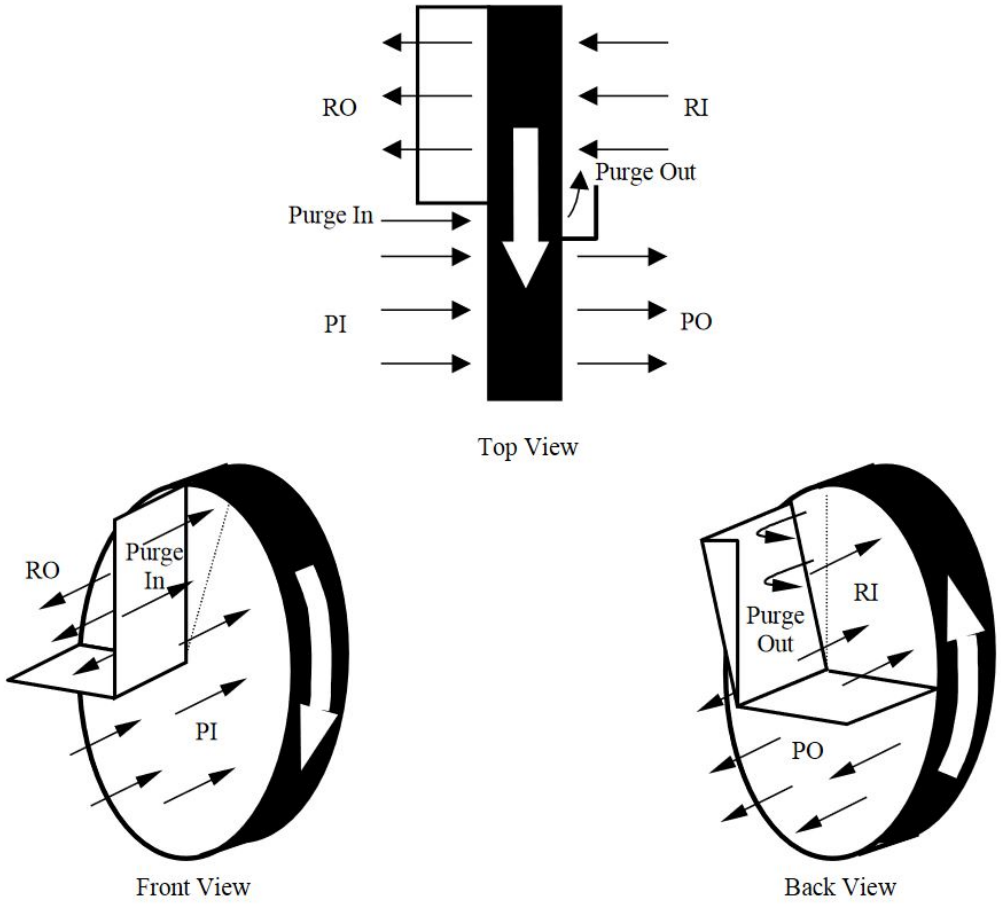

Figure 4.9: Purge section of desiccant wheel at different angles [50]

At this point of the air management system, as the process air stream enters the wheel, the air stream is divided into two; dry air stream and purge stream. The use of a purge stream has proved to improve the processed supply air quality by reducing cross-contamination. The two parameters affecting the purge flow is pressure and area. A static pressure between outdoor and return air is used as the driving force of the purge flow. It forces the contaminates of the air to the return airflow, where it gets released on the other side of the wheel as exhaust gas. The purge section area can either be fixed or adjustable and needs to be large enough to let all the contaminates through to avoid cross-contamination with the dried supply air [51]. For a higher regeneration temperature, moisture adsorption in the dehumidification process improves, but the thermal coefficient of performance decreases.

Before the return air re-enters the desiccant wheel, it goes through a loop containing a heat exchanger and a regeneration heater to conserve energy and increase the temperature of the airstream. The regeneration heater in this system reheats the airflow to 146°C [52][35], which is required to initiate the desorption process to clear the desiccant wheel. The high temperature makes it possible to store large amounts of moisture in the airflow as it exits the wheel with both moisture and other contaminants. To restore as much of the thermal energy as possible, this exhaust air exits the system through a heat exchanger, heating the subsequent purge airflow as the cycle continues. After the air stream containing the contaminates releases its thermal energy it is released as waste heat outside the factory walls. The direction of the airflows are displayed in Fig. 4.10.

4.2.4 Moisture Loads

The max moisture limit set at 0.44 gr/lb [35] moisture leaving the dry room determines the airflow through the system. Suppose the air's moisture content becomes higher than this; it will negatively affect the performance and lifetime of the batteries by reacting with the exposed material before the cells are sealed. For a dry room to function optimally, the different moisture loads in the system need to be managed. They can be divided into two main types; internal and external. Internal loads are the moisture released from inside the room from either personnel or battery material. The external is from the outside of the facility from make-up air, door openings or vapour transmission through walls, floor or the ceiling. The values for internal loads are based in the literature review [35], scaled to this factory as they are six times larger.

Internal Loads;
The first of the moisture loads are the personnel present in the dry room. Per man-hour is expected to produce 1500 grains of moisture [52][42] and with 180 workers expected to be in the room, this load amounts to 75 gr/s or 4.86 g/s.
According to [35], the moisture load from the battery material, the negative electrodes will supply a load of 2.52 g/s for a battery factory this size. The moisture content in the negative electrodes is assumed to be 0.05 wt%. This load is developed during the final drying process in the first step of the assembly stage, as displayed in Fig. 4.5.

External Loads;
The make-up airflow goes through several stages to remove the moisture content before it reaches the dry room, including cooling and dehumidification with the desiccant wheel. Ambient temperature and relative humidity are determining factors for the moisture content in the make-up air at the given site. Even if the entering airflow has an extremely low moisture content after the dehumidification processes, it adds up with the other moisture loads with approximately 0.07 gr/lb. There are some fluctuations in the overall moisture load from the dried air from the desiccant wheel, which are displayed in Fig. 4.23.

Door openings and vapour transmission provide the subsequent potential moisture loads. By purging airlocks with dry room air, moist outside air is removed from the door openings. Positive pressure inside the room keeps the outside air away from the entryway to the room. making it approximately unaffected by the outside climate. The same can be

said for vapour transmission through walls, floor and ceiling. The construction process and technology of the dry rooms of today prevents this from being a factor. For these reasons, this moisture load can be neglected as the dry room is practically isolated from the outside conditions.

4.2.5 Air Mass Flow Calculation

The air mass flow rate required through the dry room can be calculated using eq.(4.2) [53]. This is the required amount of air to remove a given amount of moisture from an environment. The calculations take into account the inlet moisture loads and a set limit for the humidity ratio of the air inside the dry room. The mass flow rate calculated is the required circulation of air to maintain a moisture content at a set limit.

$$\dot{M} = \frac{G}{(x_r - x_a)} \tag{4.2}$$

Where:
$\dot{M}$ = Mass flow air, kg/s
G = Moisture load, kg/s
x_r = Humidity ratio room, kg moisture/kg air
x_a = Humidity ratio inlet air, kg moisture/kg air

For this system, the set value will be the humidity ratio in the room, x_r, that controls the mass flow. This represents the moisture content of the outlet air of the dry room, and should have a constant value of 0.44 gr/lb to keep the air quality of the dry room. The other values are changing constantly, depending on the conditions in the system.

4.3 Simulink Model

The air management system is created using a Matlab/Simulink environment. The programs works together to create and customize multiple different types of systems. Simulink creates a physical model with graphical programming, while the Matlab environment is the textual part where data sets are imported, and simulations can be visualized. By running simulations in the initial stage of a project, risk and cost can be reduced as the simulations can accurately emulate the actual conditions. Testing different methods and approaches will reveal the optimal solutions. In some cases, a generic model of a given system can be accessed and customized by adding known parameters and values. It is also possible to build the model from scratch, such as this system has been. Simulink has been the primary simulation tool in this thesis, using the physical model of the system to simulate the results.

Fig. 4.10 shows a flow chart describing the air management system following the direction of the airflow through the simulation model. The details for each of the major components will be described in this section.

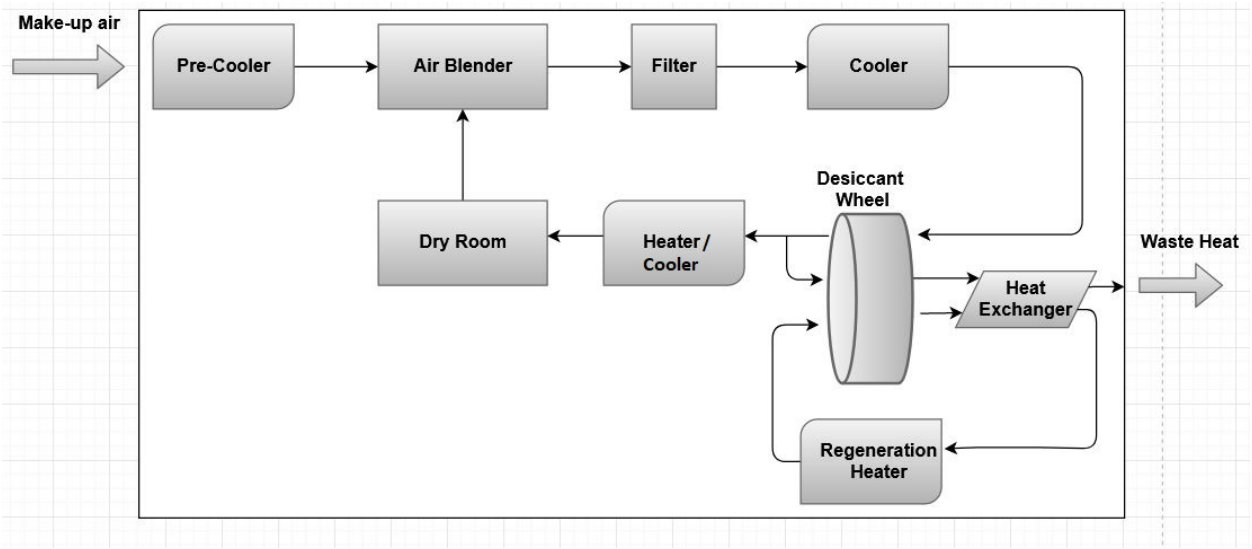

Figure 4.10: Schematic of the air management system for the dry room

4.3.1 Simulation Strategy

The Simulink model uses two main input parameters; make-up air temperature and relative humidity. The objective is to simulate the air management system during the conditions for an entire year. Ambient conditions follow the seasonal fluctuations and to determine how the system responds to these; a one-year simulation will be conducted. The total simulation time is 1200 seconds, with each 100-second interval representing one month, starting in January.

Each of the temperature control units has temperature limits, using a previous study of a dry room [35] for the baseline values. By testing, these values have been altered and customized to optimize the given system for the ambient conditions, expected loads and to maintain within some given limits. For more preferable conditions than the limits, for example, lower temperatures air entering a cooler, it passes through a switch without any changes.
The moisture controller in the dry room uses a reactive feedback loop to correct the actual value to the target limit. This limit, set at 0.44 gr/lb or 100 PPMV dry air, controls the mass airflow through the room. 100 PPMV results in a dew point of -42°C with a relative humidity of 0.410%, shown in Table B.1. In this case, the moisture limit is a set value, where higher and lower values will be corrected to maintain stable conditions. Higher moisture content in the room will demand a higher air mass flow to keep the moisture content at the desired level following eq. (4.2). For conditions where the moisture content is below the limit, the mass flow is reduced to keep the moisture level constant. There is a direct correlation between inlet make-up air and air mass flow, as the purge rate is fixed. Due to this relationship, unnecessary high mass flow will result in more energy spent on temperature controlling and dehumidification of make-up air.

4.3.2 Input Values

The input values for the simulation are the make-up air temperature and its relative humidity. These values will vary according to the ambient conditions at the factory site.

For Arendal, the average temperature and relative humidity for each month during a year are displayed in Figs. 4.2 and 4.3. These values are used in the simulation. The actual input signals used in the simulations are presented in Figs. 4.11 and 4.12.

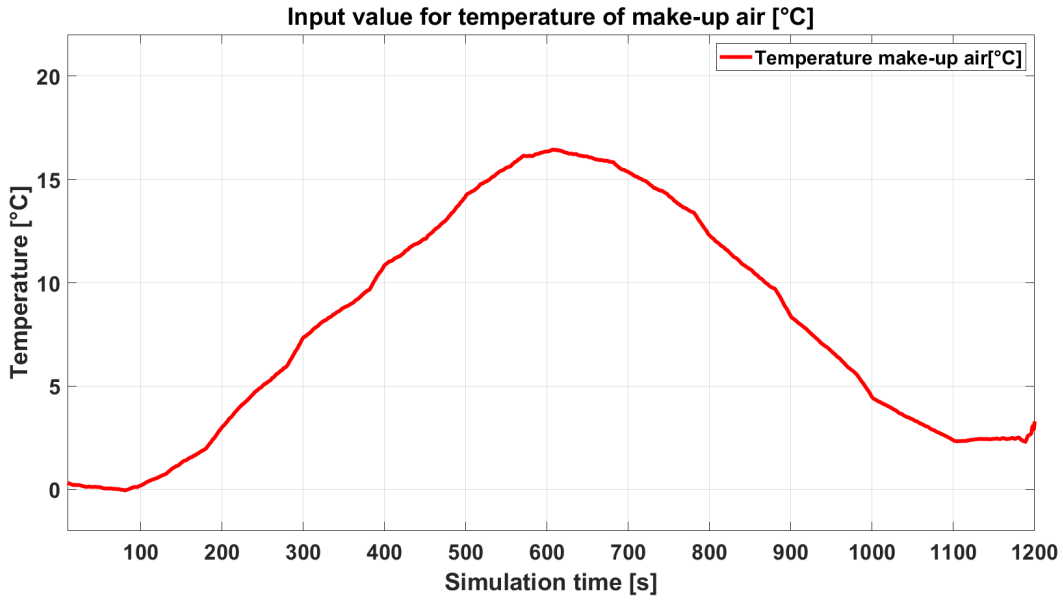

Figure 4.11: Temperature make-up air

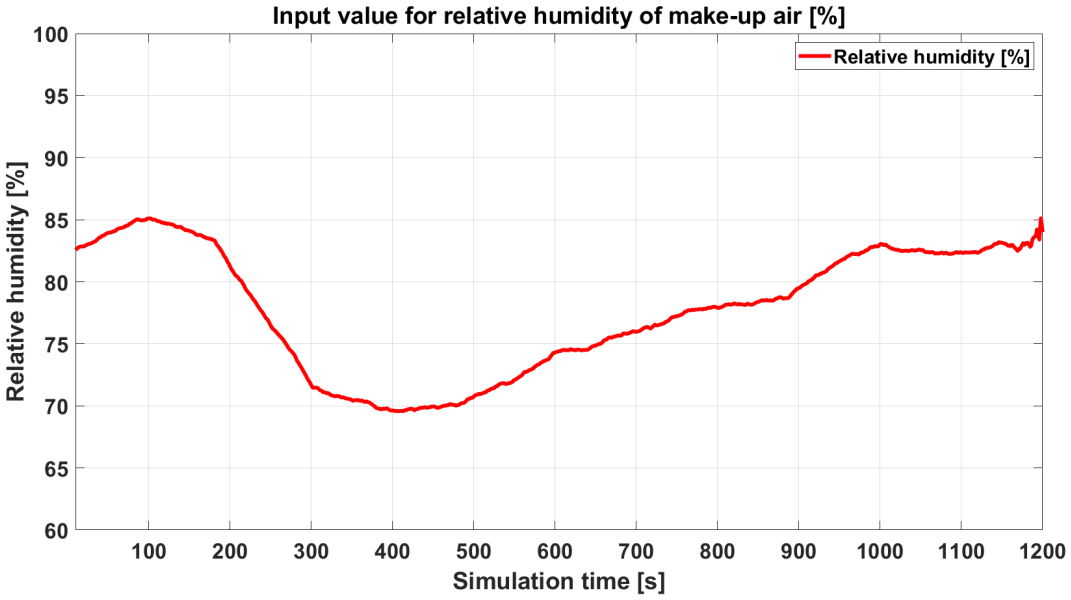

Figure 4.12: Relative humidity make-up air

The coolers' temperatures limits are determined based on the overall power demand and used as an indicator for the optimal temperatures. The initial values are based on the literature review and tested with a +/- 3°C, from the 9°C for the pre-cooler and 13°C for the cooler. Table 4.3.2 shows the result of the simulations to deciding the new temperatures of these two units.

Table 4.1: Simulation results for cooler temperatures

Pre-cooler [°C]	Cooler [°C]	Power [kW]	Mass flow [kg/s]
9	10	4806	173.5
9	13	4901	180.9
9	16	4895	183.5
6	10	4562	165.6
6	13	4676	174.0
6	16	4648	175.3
12	10	5069	182.0
12	13	5130	187.8
12	16	5177	192.7

The power demand of the overall system is at its lowest when the two coolers operate at a higher capacity, cooling the air to 6°C for the pre-cooler and 10°C for the cooler. Even if there is a higher power demand for cooling the air, the air mass flow is reduced by removing moisture from the mechanical dehumidifier. Another benefit of this structure is that the power demand and mass flow gets a more stable profile with less seasonal fluctuation due to more constant inlet moisture. The results of these simulations are not the final values used as other parts of the system has been changed. It is only used to determine the temperatures based on the lowest power demand.

4.3.3 Pre-Cooler

The pre-cooler will function as a mechanical dehumidifier by reducing the make-up air temperature to reduce the moisture content. The desired upper limit for the outlet temperature is 6°C, but a lower temperature will pass through a switch unchanged. Fig. 4.13 shows the pre-cooler subsystem with temperature and relative humidity as inlet values from the ambient conditions of the make-up air.

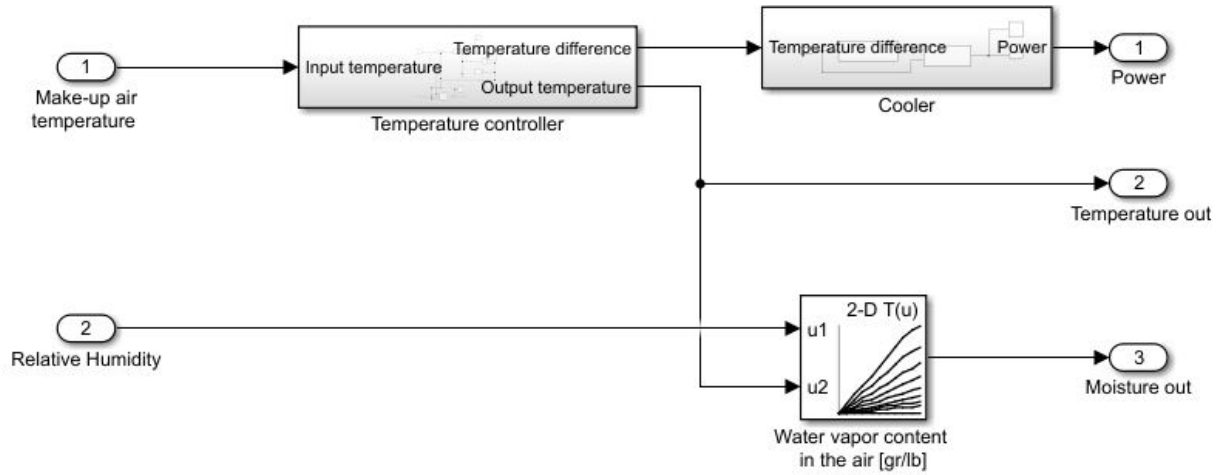

Figure 4.13: Control systems and cooling unit for the pre-cooler

The temperature controller system in Fig. 4.14 uses the desired output temperature set at 6°C and a PID controller to adjust the actual temperature to the desired. All the con-

trollers in the system use a closed-loop for the simulations. As the desired value used in the control system is a max limit, a switch is incorporated. This ensures that values lower than the limit will not enter the control loop and remain the original value as it is even more desirable. There will be a temperature difference between the input and output for the temperatures adjusted by the controller. This value is used to calculate the power required to achieve this temperature for the airflow.

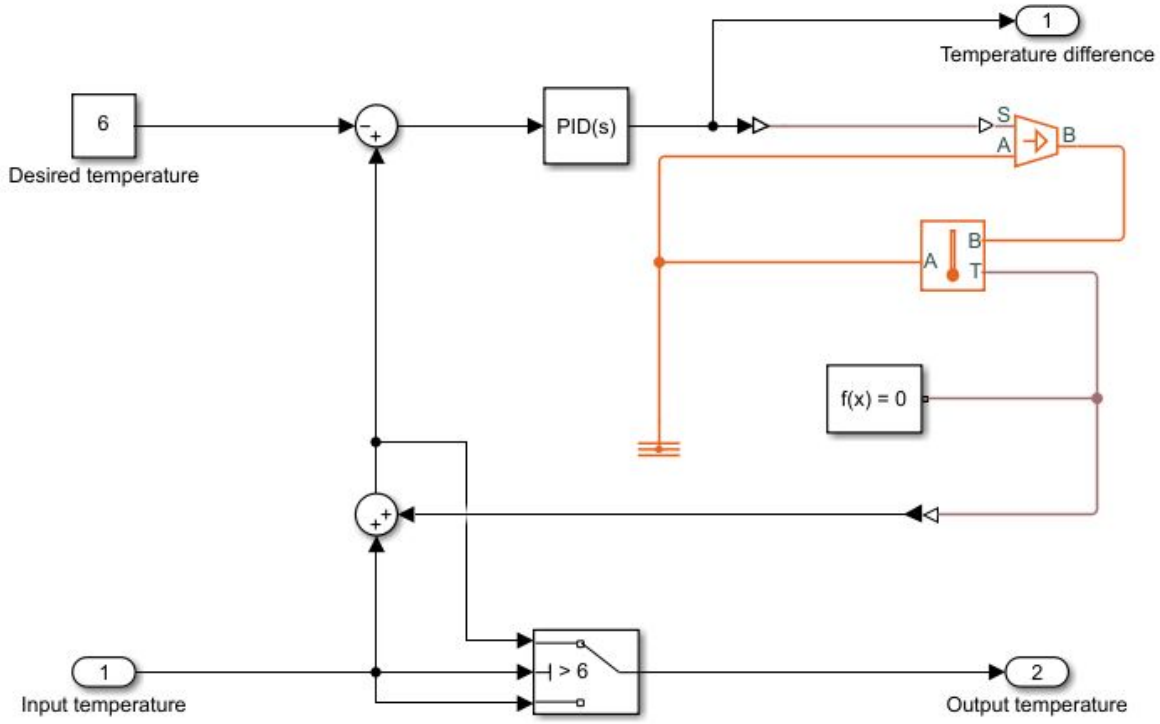

Figure 4.14: Temperature controller for pre-cooler

The outlet temperature from the temperature controller is used in a lookup table for moisture content in the air. These values are from Table 4.2, following the Mollier diagram [34][54]. The moisture content selected from this table by assuming the same relative humidity as the ambient conditions for the cooled air, depending on input temperature and relative humidity. The temperature is given within the range of -1 to 38°C and the relative humidity from 0 to 100%. Output values are determined by interpolating between the table values for changing input, and given as grains moisture per pound dry air (gr/lb).

Table 4.2: Moisture content in air depending on relative humidity and temperature during standard atmospheric pressure [54]

Relative Humidity [%]	Temperature [°C]								
	-20	-1	4	10	16	21	27	32	38
0	0	0	0	0	0	0	0	0	0
10	0	3	4	6	8	11	16	21	29
20	0	5	7	10	16	21	30	42	58
30	0	7	11	14	22	34	46	65	87
40	0	9	14	20	30	44	62	85	116
50	0	12	18	26	39	55	78	108	147
60	0	14	22	32	48	66	92	128	176
70	0	17	26	38	54	78	108	152	208
80	0	19	29	42	62	88	125	173	234
90	0	21	33	48	70	100	140	190	258
100	0	23	37	56	79	114	156	208	273

Fig. 4.15 shows the moisture content of the outlet air from the pre-cooler before it enters the air blender.

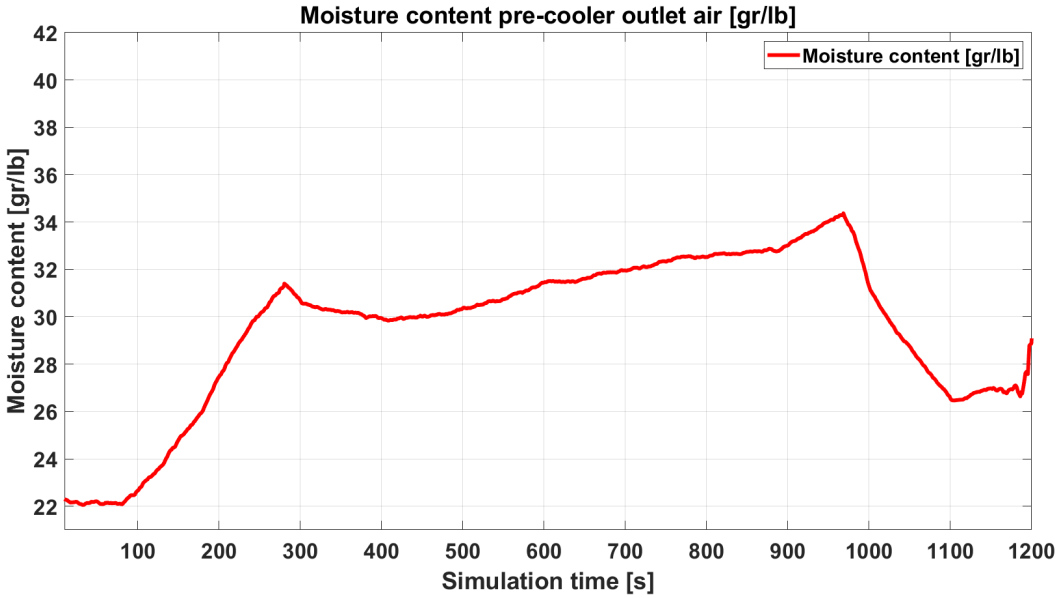

Figure 4.15: Moisture content out from pre-cooler

The cooler subsystem is used to determine the power demand for the temperature control of the air. Inside the cooler subsystem, there are two main parts showed in Fig. 4.16; a thermostat and a cooler. The thermostat uses a relay with an on/off switch, dependent on a positive temperature difference. In this case, the output signal will be 1, representing a turned on cooler. For temperature differences of 0 or a negative value, the switch is turned off.

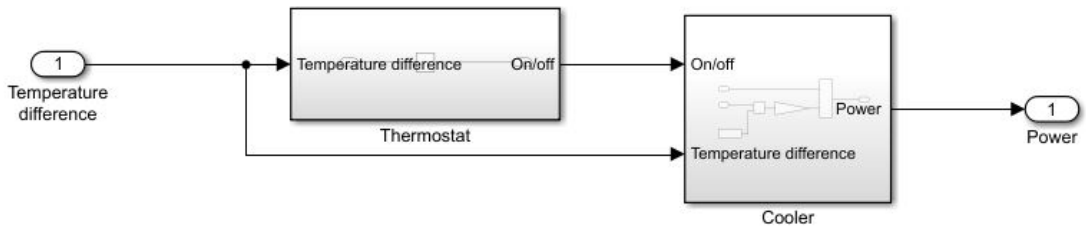

Figure 4.16: Inside the cooler subsystem

The cooler operates following eq. (2.8), combined with the on/off signal from the thermostat. Fig. 4.17 shows the cooler block where the temperature difference is multiplied with the mass flow, specific heat for air, mass flow and purge rate of the air. The mass flow will be calculated in the dry room section, as it depends on the moisture content in the room. This value is constantly changing as it adapts to the given conditions in the dry room to reduce energy demand while maintaining the required conditions.

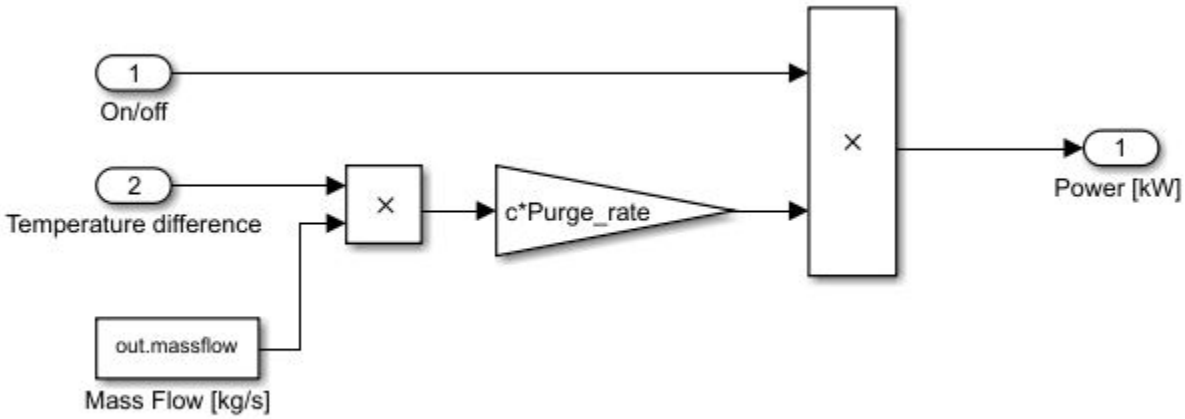

Figure 4.17: Power calculations pre-cooler

4.3.4 Air Blender

The air blender operates as an economiser by mixing two airflows, inlet make-up air and outlet dry room air. The make-up air is proportional to the purge rate, which is equal to 8.17% of the overall mass flow. The remaining 91.83% is the outlet from the dry room called the reuse rate. This airflow is reused in the air management system and blended with the new airflow from the input make-up air. Fig. 4.18 displays this system in the Simulink model, where the gains represent the reuse and purge rate.

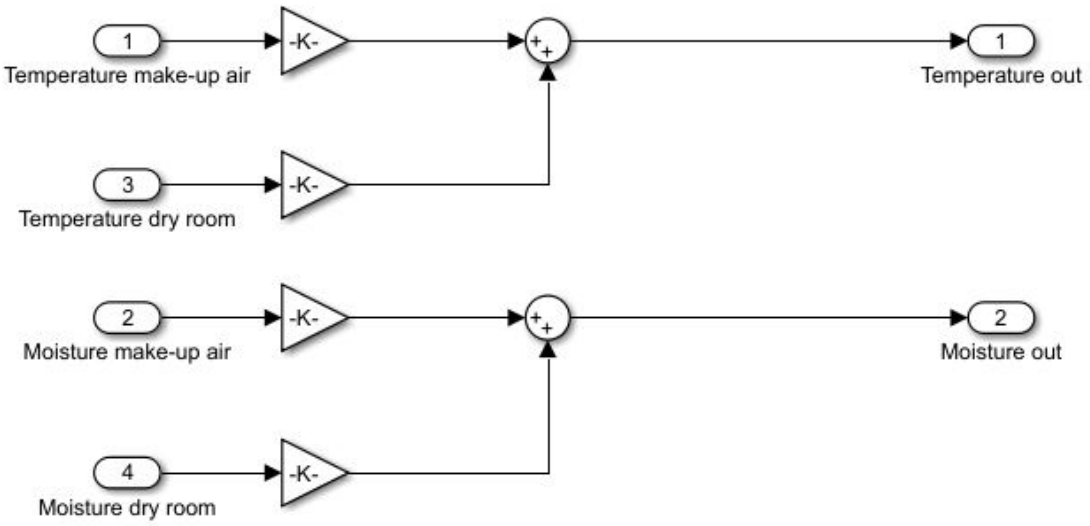

Figure 4.18: Air blender mixing airflows from pre-cooler and dry room

The temperature and moisture content outlet values from the air blender are displayed in Figs. 4.19 and 4.20.

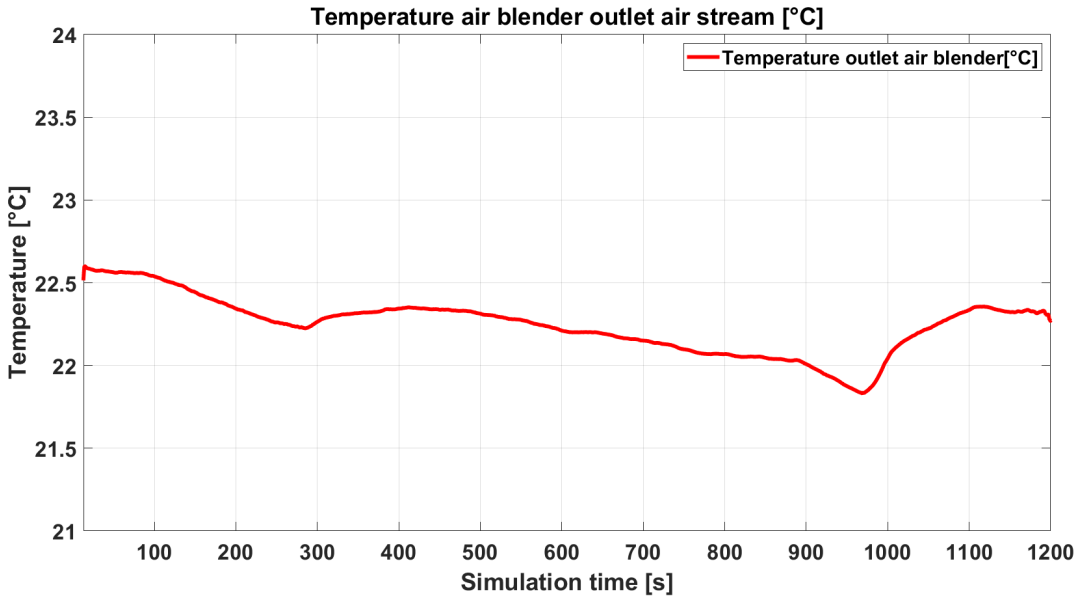

Figure 4.19: Temperature of the outlet air from the air blender

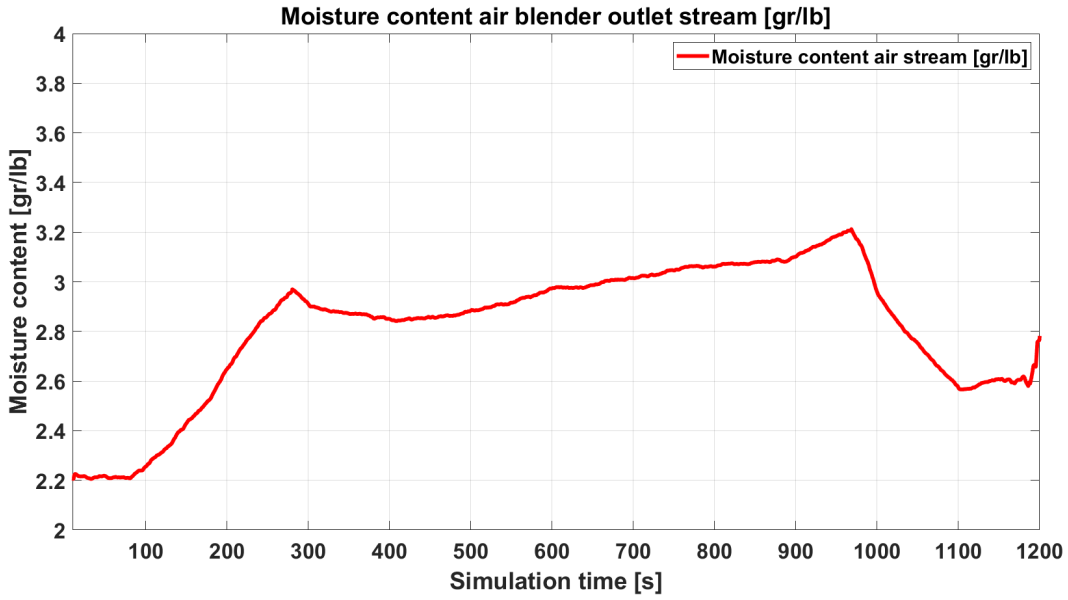

Figure 4.20: Moisture content of the outlet air from the air blender

4.3.5 Desiccant Dehumidification Wheel

The simulations of the desiccant wheel is conducted using a simulation software from NovelAire [55]. As the desired outlet moisture content for a dry room is very low, a 3:1 spilt between process and regeneration area is used with a high regeneration temperature. The two airflows uses a counter flow and a high temperature regeneration heat airflow at 146°C. The simulation model is displayed in Fig. 4.21, using the expected inlet parameters of 10 °C and 3 gr/lb for air temperature and moisture content of the air.

The inlet temperature and moisture content of the air will deviate from earlier described and expected values of 10°C and 3 gr/lb during the simulation. Therefore, different values have been simulated during the otherwise equal settings to cover a broad spectre of inlet conditions. The inlet temperature has been tested for 0-30°C with a moisture content between 0-10 gr/lb, with a constant regeneration temperature at 146°C. The results of the simulations are displayed in Table 4.3, which are used in a lookup table in the Simulink model. The outlet values will be interpolated depending on the two inlet values, providing the outlet moisture content from the desiccant wheel.

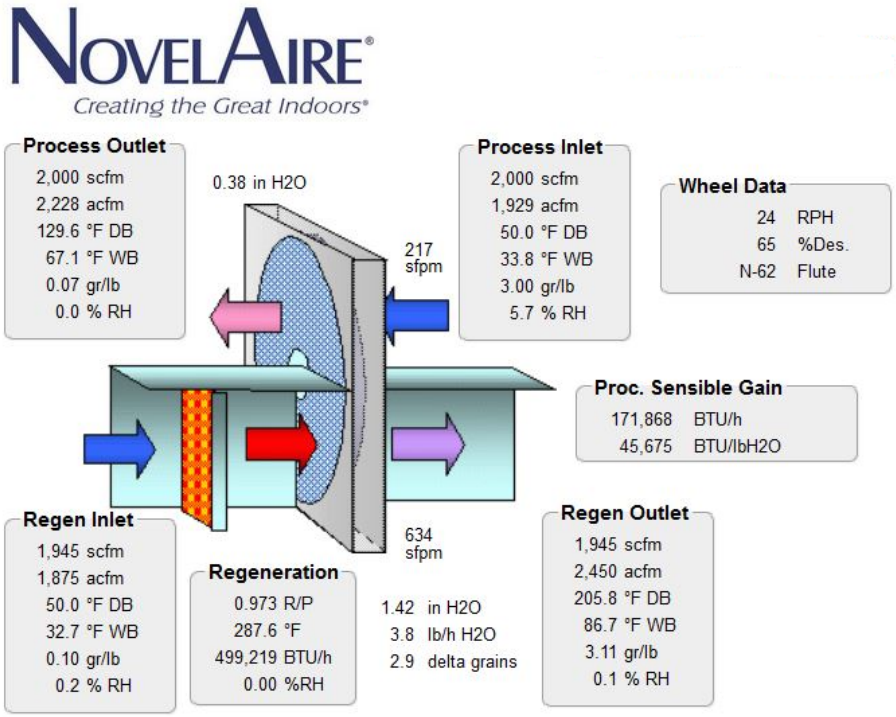

Figure 4.21: Simulation tool from NovelAire for the desiccant wheel [55]

The model is validated as the results correspond with the results from the literature review. The simulation results gives 0.07 gr/lb for the same inlet conditions, 10°C and 3 gr/lb, where the study from the literature reviews value is 0.066 gr/lb.

Table 4.3: Simulation results for desiccant wheel

Temperature [°C]	Moisture content [gr/lb]							
	0	1	2	3	4	5	6	10
0	0	0.02	0.04	0.07	0.10	0.10	0.12	0.17
6	0	0.03	0.05	0.07	0.09	0.11	0.14	0.22
8	0	0.03	0.05	0.07	0.09	0.12	0.14	0.23
10	0	0.03	0.05	0.07	0.10	0.12	0.14	0.24
12	0	0.03	0.05	0.08	0.10	0.12	0.15	0.25
18	0	0.03	0.06	0.08	0.11	0.14	0.17	0.28
30	0	0.04	0.07	0.11	0.15	0.19	0.23	0.40

The Simulink subsystem of the desiccant wheel is shown in Fig. 4.22. The two inputs used in the lookup table of the desiccant wheel simulation are temperature and moisture content of the air stream.

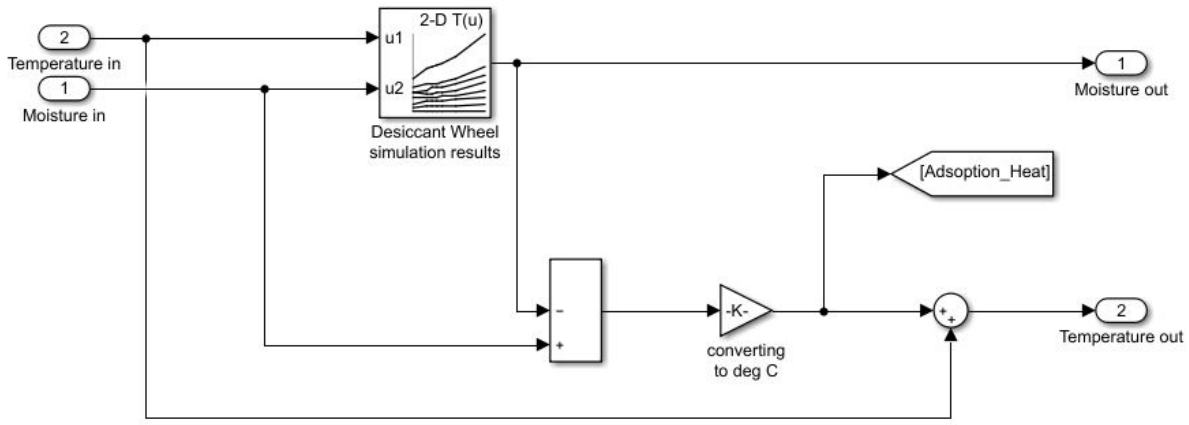

Figure 4.22: Simulink system of desiccant wheel

The moisture content of the outlet air from the desiccant wheel is presented in Fig. 4.23. The outlet moisture content from the desiccant wheel will be affected by the inlet moisture of the air, so if a lower moisture content were needed, a more thorough pre-drying process would be required. This will increase the power demand of the overall system.

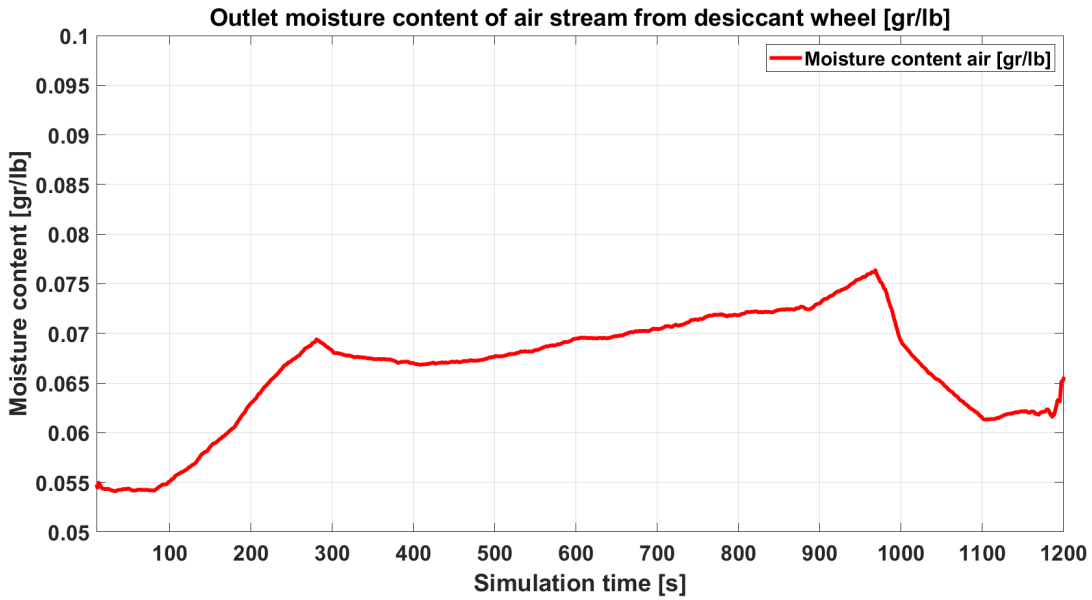

Figure 4.23: Moisture content of outlet air from desiccant wheel

During the moisture adsorption process by the molecular sieve in the desiccant wheel, adsorption heat is released in an exothermic reaction. The amount is calculated using eq. (4.1) and converted to °C before adding it to the inlet temperature. The same process is reversed to an endothermic reaction during the desorption process, where the moisture is released from the molecular sieve. This process is drawing the same temperature

from the regeneration air stream later in the process as is supplied to the process air. Fig. 4.24 shows the graph of the adsorption heat, given in °C, correlates to the amount of moisture adsorbed by the molecular sieve. The adsorption heat averages 5.16 °C, with the same seasonal changes as the moisture content in the system.

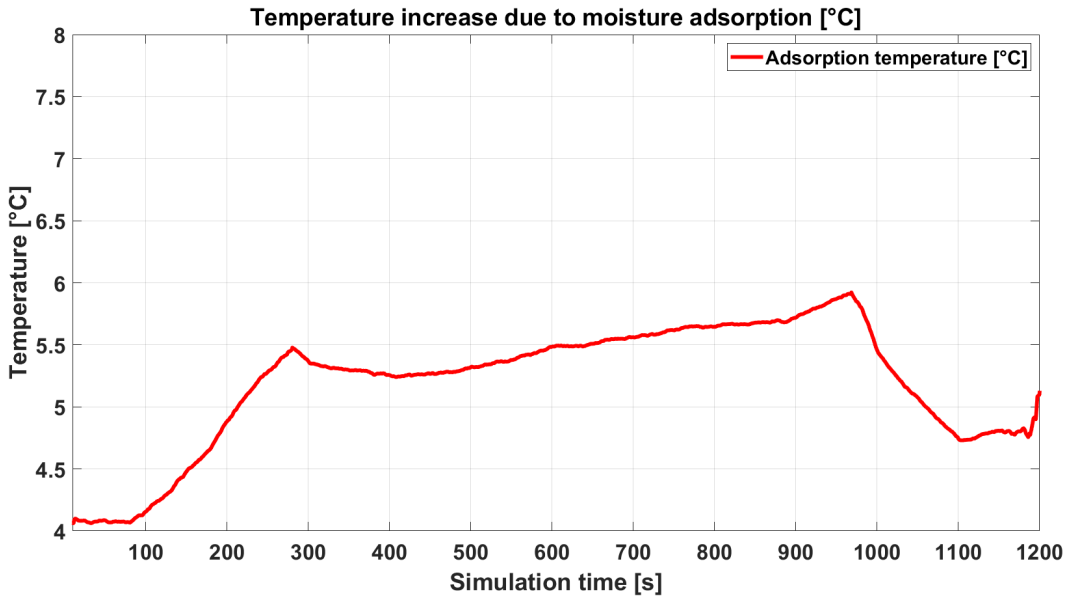

Figure 4.24: Heat from adsorbing moisture with the desiccant wheel

4.3.6 Heat Exchanger

Helical coiled heat exchangers, a compressed shell and tube heat exchanger are commonly used for heat, ventilation and air conditioning (HVAC) applications due to the high heat transfer rate and compact size. The addition of centrifugal forces created by the helical structure generates a secondary flow. This flow is normal to the original flow and causes increased friction and heat transfer rate [56]. Therefore, this is the heat exchanger type selected for this project. The two airflows are never in direct contact to avoid cross-contamination of impurities, and only thermal energy is transferred between them.
The cost, both investment and O&M, for a heat exchanger largely depends on the size given as heat transfer area. Eq. (4.3) [57] is used to calculate the overall cost of the heat exchanger through the expected lifetime. The study used to develop this equation looked at heat exchangers with a given heat transfer range 0.5 m^2 < S_{hts} < 47 m^2.

$$C_{hts} = 55\,S_{hts} + (78 S_{hts})\,a \tag{4.3}$$

Where:
S_{hts} = Heat transfer area, m^2
C_{hts} = Investment and operation cost heat exchanger through expected lifetime, €
a = Lifetime heat exchanger, years

The objective of the heat exchanger is to recycle the heat in the system for further use. The regeneration airflow used for the desorption process of the desiccant wheel, T_d, is lead into the heat exchanger where it heats the incoming purge airflow, T_{in}. On the way out of the desiccant wheel, the air transports the moisture content and other contaminants/impurities from the wheel and releases it with the discharged airflow waste heat, T_w. Fig. 4.26 shows the inside of the heat exchanger subsystem, containing two new subsystems for heat transfer rate and heat energy balance. Each airflow is the same size as the purge airflow and operates in a continuous cycle. Fig. 4.25 shows the schematics of the heat exchanger used and the directions of each of these airflows.

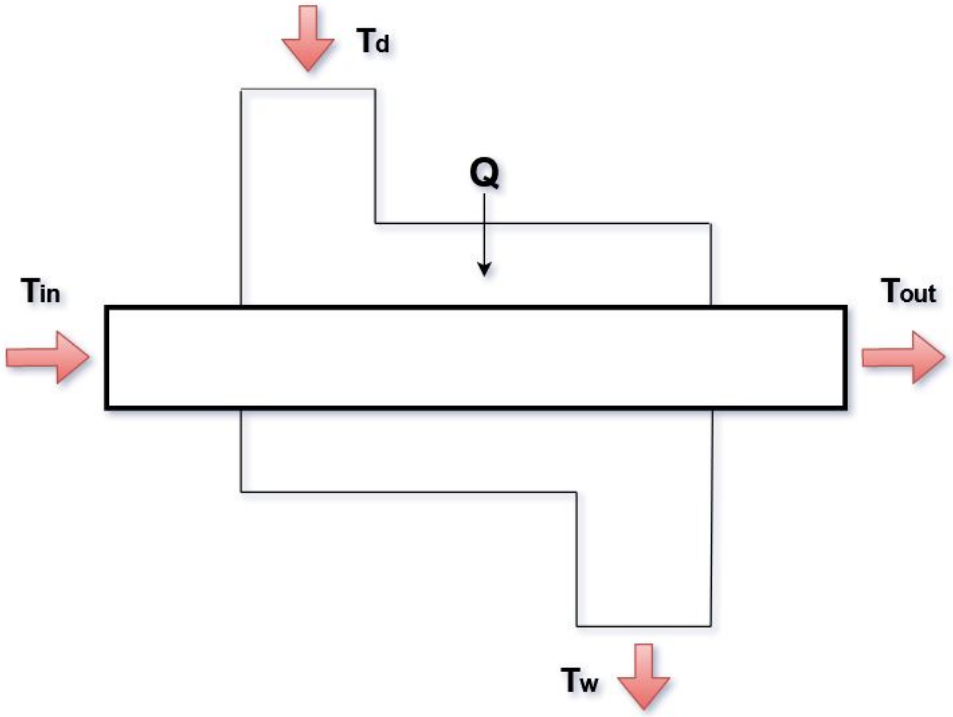

Figure 4.25: Heat exchanger schematics

T_{in} = Inlet temperature from purge section, to heat exchanger
T_{out} = Outlet temperature from heat exchanger, to regeneration heater
T_d = Inlet temperature from desiccant wheel containing contaminates
T_w = Outlet waste heat temperature

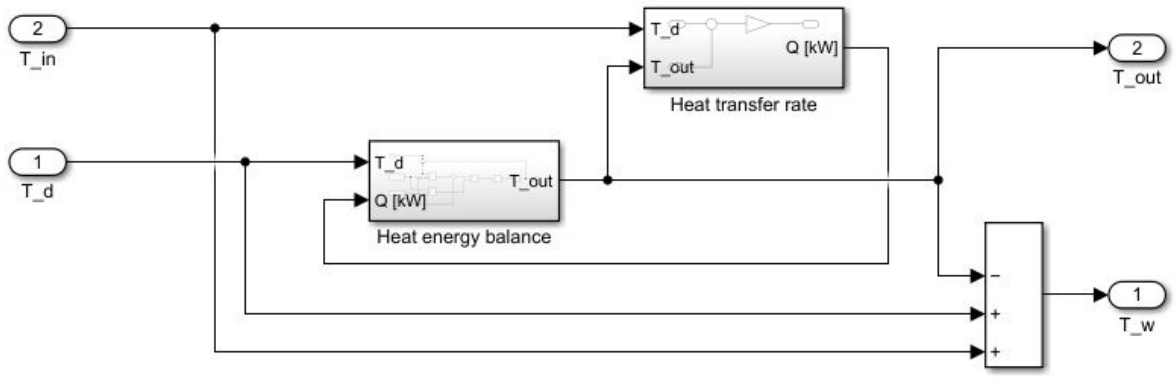

Figure 4.26: Heat exchanger subsystems

Figs. 4.27 and 4.28 show the inside of the subsystems temperature change and heat transfer rate, following eq. (2.8) to calculate the outlet temperature from the heat exchanger. The heat transfer rate depends on the temperature difference between the hot air and the actual output air temperature from the heat exchanger and the UA-value. The overall heat transfer coefficient is set to the middle of the spectre for forced convection heat exchanger gasses at 20 W/m^2K, which can be in the range of 10-30 W/m^2K according to [32].

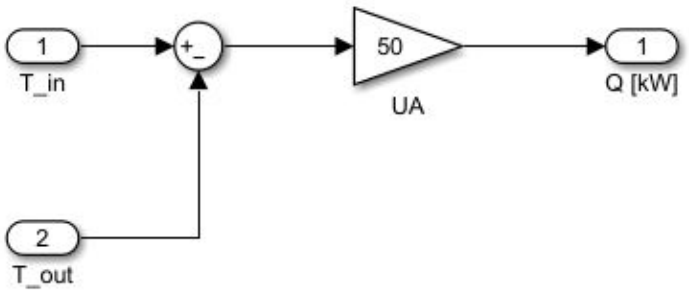

Figure 4.27: Heat transfer rate calculations

Eq. (4.4), a modified version of eq. (2.8), shows how the heat energy balance has been calculated [58]. The energy balance calculations show the temperature change of T_{out} with respect to the simulation time.

$$\dot{m}\, C_p \frac{dT_{out}}{dt} = \dot{m}\, C_p\,(T_{in} - T_{out}) + Q = \dot{m}\, C_p\,(T_{in} - T_{out}) + UA\,(T_d - T_{out}) \qquad (4.4)$$

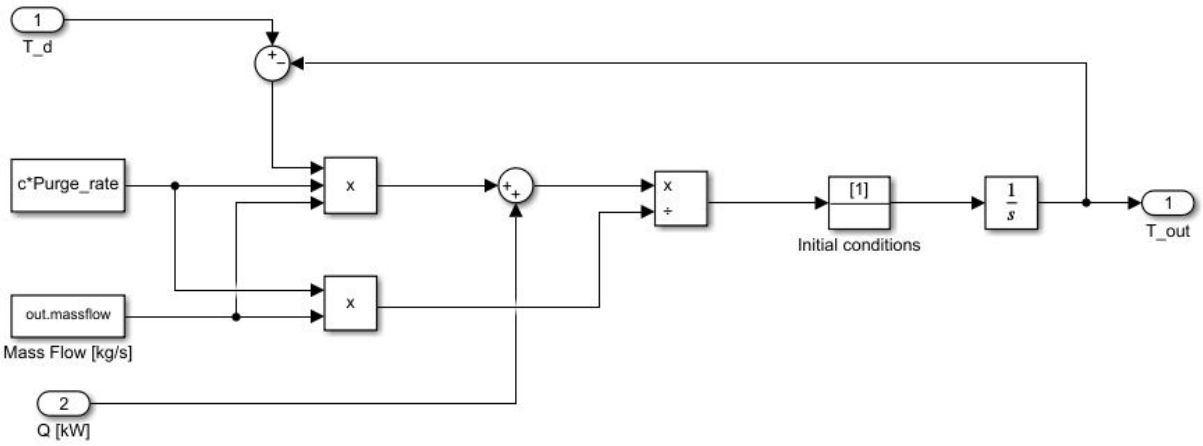

Figure 4.28: Heat energy balance calculations

4.3.7 Temperature controlling units

The three remaining temperature controlling units, cooler, regeneration heater and heater/cooler, operate similarly to the pre-cooler. The actual Simulink blocks are not displayed, but the differences are described below.

Cooler

The cooler reduces the temperature of the inlet air stream to 10°C due to the simulation results displayed in Table 4.3.2. It operates similarly to the pre-cooler explained in Section 4.3.3. The cooler uses 100% of the airflow, given that it is placed between the air blender and the desiccant wheel, where the airflow splits into purge and process air streams.

Regeneration heater

The purged airflow that exits the heat exchanger enters the regeneration heater. The objective of the regeneration heater is to re-heat the purged airflow to be used for the desorption process of clearing the desiccant wheel before the next revolution. The airstream will lose some heat from this process, proportional to the adsorption heat before it enters the heat exchanger again. This time it contains moisture and other contaminants that will be released as waste heat on the other side of the heat exchanger. Without the distinct difference that the heater heats the airflow, it functions in the same way as the cooler. The desired temperature is 146°C, using the purge rate airflow.

Heater/cooler
Following the desiccant wheel, another heater/cooler is used to control the airflow before it enters the dry room. The outlet temperature from the dry room should be between 22 and 25°C. This is achieved by setting a temperature range of the dry room inlet air between 12 and 14°C. There is another constant heat load inside the dry room, which will be explained more in the following subsection. By factoring in this and the changing mass flow, the temperature range set will maintain the desired temperature of the air inside the dry room. For the conditions in this simulation, the temperature controller will only need to operate as a cooler. However, if the inlet conditions of this unit were to drop below 12°C, the heater would begin operating on the air flow.

4.3.8 Dry Room

The dry room subsystems are divided into two main parts; Fig. 4.29 shows the temperature calculations and Fig. 4.30 the moisture control and mass flow calculations. The constant values used in the dry room simulation, heat and moisture loads, are from the literature review and scaled up to six times their original value, proportional to this factory size.

The air temperature inside the dry room is not actively heated but will experience a temperature rise due to heat from equipment and personnel. For a dry room of this size, the heat load is expected to be equivalent to 1,500 kW working on the air. Following eq. (2.8) the outlet temperature of the dry room air is calculated and displayed in Fig. 4.29.

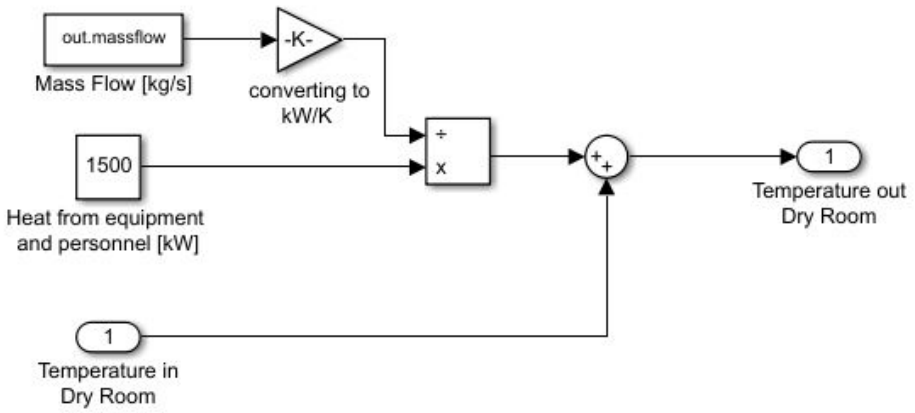

Figure 4.29: Dry room temperature calculations

Fig. 4.30 shows the dry room moisture control and air mass flow calculations. Three main moisture loads contribute to the air inside the dry room; personnel, the batteries' negative electrode, and the dry input air from the desiccant wheel. These are used as the input values used to determine the outlet moisture content and required air mass flow rate.

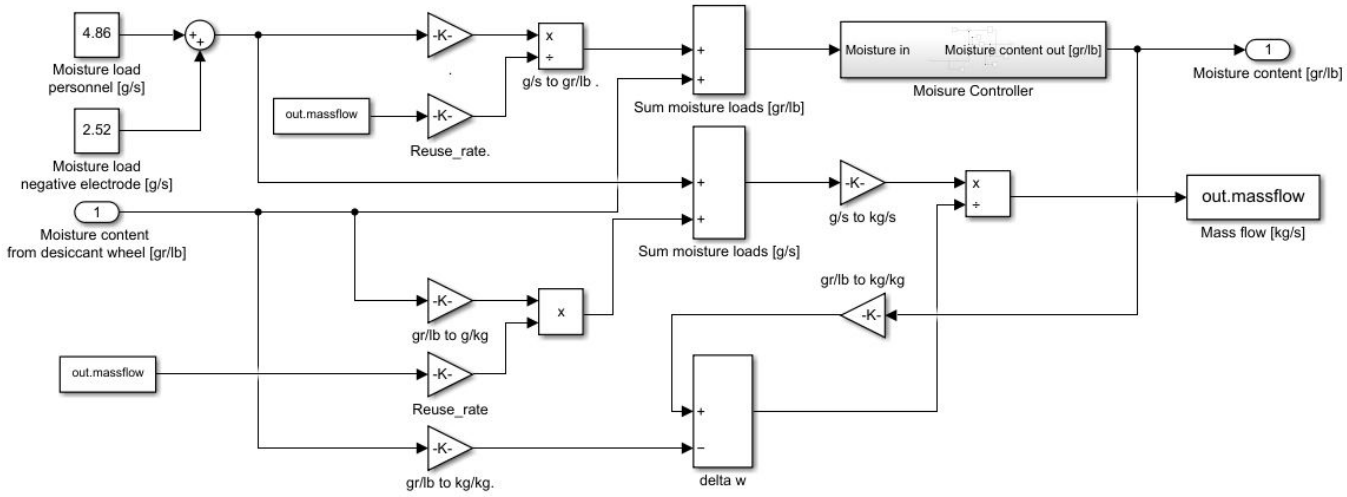

Figure 4.30: Dry room moisture loads and air mass flow calculations

The moisture load from personnel and negative electrodes are estimated to be 4.86 g/s and 2.52 g/s. These values are averages, as the dry room is assumed to operate at a constant capacity. The final moisture load is from the dried air from the desiccant wheel. Even if the moisture content in this air is low, it will add to the existing moisture in the dry room environment, especially when the air mass flow is large. Due to airlocks surrounding the air and vapour proof perimeter, moisture from transmission through walls and door openings are neglected in this thesis. The gains used in the Simulink models are used for converting between different units, as described in the given figures.

Following eq. (4.2), the mass flow rate of the air through the dry room is calculated. As it depends on the moisture load supplied in the room and the actual moisture content in the air, this flow rate will change to reduce the required power demand whilst maintaining sufficient air quality. The determining variable is the limit for moisture content in the dry room, set to be 0.44 gr/lb. This is regulated using the moisture controller subsystem, displayed in Fig. 4.31 where a PID controller is used to keep this value constant. Variation in temperature and moisture inside the dry room will cause reduced quality of the battery cells and should therefore be avoided.

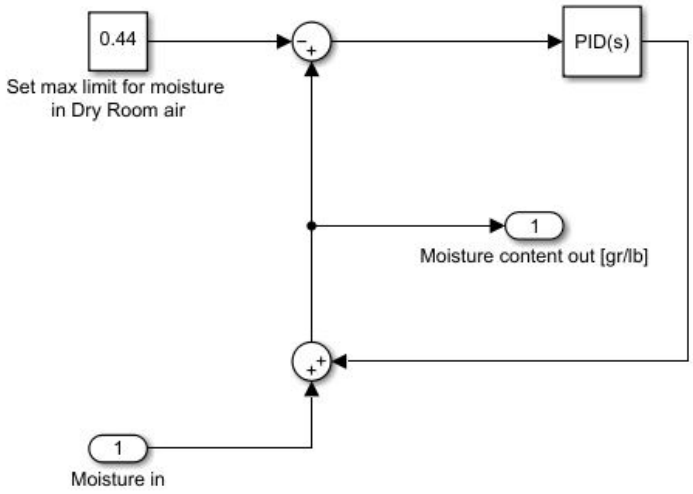

Figure 4.31: Dry room moisture controller

4.4 Sizing of Heat Exchanger

Multiple simulations with different UA-values has been conducted to determine the optimal composition of heat exchanger size. Changing the size of the heat exchanger will also impact the waste heat temperature, as it depends on the heat transfer area of the heat exchanger. With the overall heat transfer coefficient assumed to be constant 20 W/m^{2}K for forced convection heat exchanger gasses, the only changeable parameter is the heat transfer area.

The prices in the results are given in NOK with a conversion rate where 1 € = 10 NOK [59]. Power-intensive industry usually uses get their electricity through fixed-price contracts, assuring a more stable cost. The average prices for these types of Norwegian industries in 2020 paid, excluding fees and grid rent, 0.284 NOK/kWh [60].

Eq. (4.3) is used to calculate the investment and O&M cost of the heat exchangers through its expected lifetime. According to the study that created the price formula, the lifetime for heat exchangers such as this is set to be 10 years [57]. Some uncertainties are using this formula, as it has been created using many different types of heat exchangers for various conditions. One of the largest operating cost is cleaning, where the paper states that cleaning due to contamination is done up to three times each year. There are few chemical contaminants for the dry room application compared with other applications. Therefore, it is assumed only to clean the heat exchanger once each year, reducing this cost to a third. This gives the updated formula (4.5).

$$C = 55\, S_{hts} + \left(78\, S_{hts}\, \frac{1}{3}\right) a \tag{4.5}$$

Where:
C = Total cost heat exchanger, €

The overall cost covers the total cost of the heat exchanger and the cost of the power demand for the regeneration heater. The results of the simulation, in terms of waste heat temperature, required power from regeneration heater, and the overall cost, are presented in Table 6.1. These values are used to create Fig. 6.3, displaying the comparison between waste heat temperature and cost for regeneration power. The overall cost of this part of the system is used to determine the optimal size of the heat exchanger. This is an isolated part of the overall system given that the regeneration heater is required to supply 146°C regardless of the other conditions. With a larger UA-value, giving the heat exchanger a larger heat transfer area, it can adsorb more heat and reduce the waste heat temperature and power demand. However, with a larger heat exchanger there are more investment and operation cost.

4.5 Sensitivity Analysis

Although the annual averages of temperatures and relative humidity are predictable, it is important to determine how vulnerable the system is to changes to the input variables. Creating different scenarios with changing parameters will expose potential weaknesses and determine how different factors impacts the system. The different scenarios will be compared with the original simulation, referred to as Baseline.

Scenario 1 has an average increase of input values of 5%, while Scenario 2 has a decrease of 5% to determine the impact different ambient conditions will have on the system. The input signals are displayed in Figs. 4.32 and 4.33.

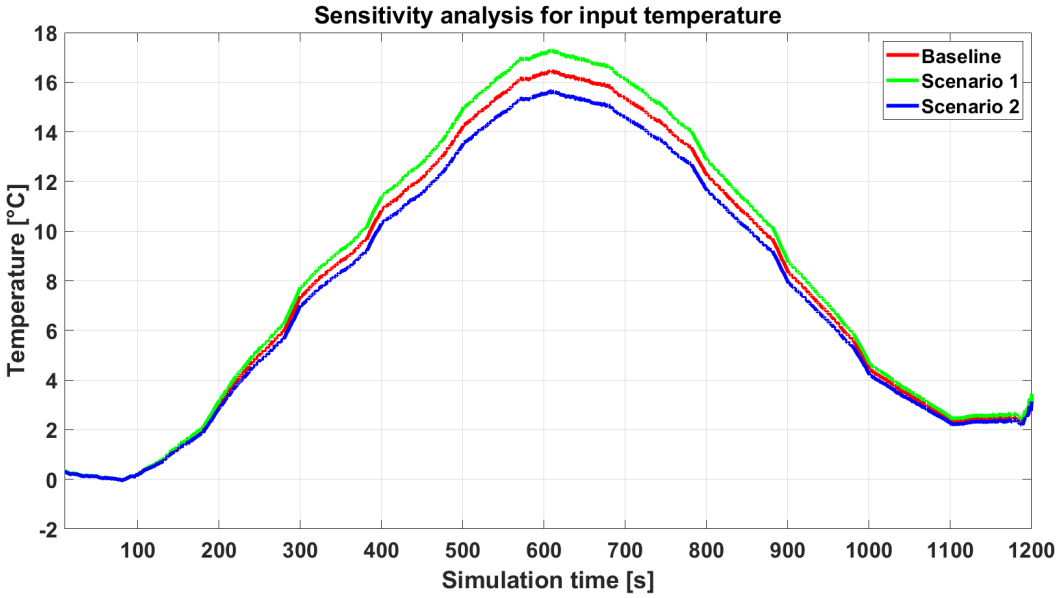

Figure 4.32: Input temperatures for sensitivity analysis

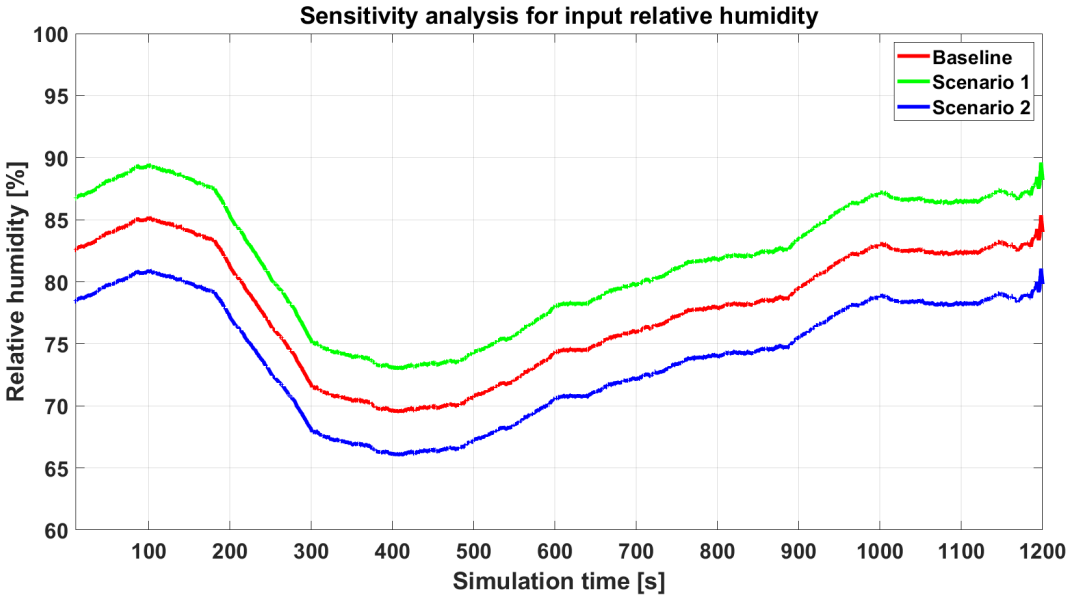

Figure 4.33: Input relative humidity for sensitivity analysis

To determine any impact of the system for inconsistencies in the average temperature and relative humidity values, Scenario 3 has a random percentage in the range +/- 10% of the Baseline. These input signals are displayed in Fig. 4.34. The values follow the seasonal trend with the same annual average, but with a more significant deviation from the mean value from each data point.

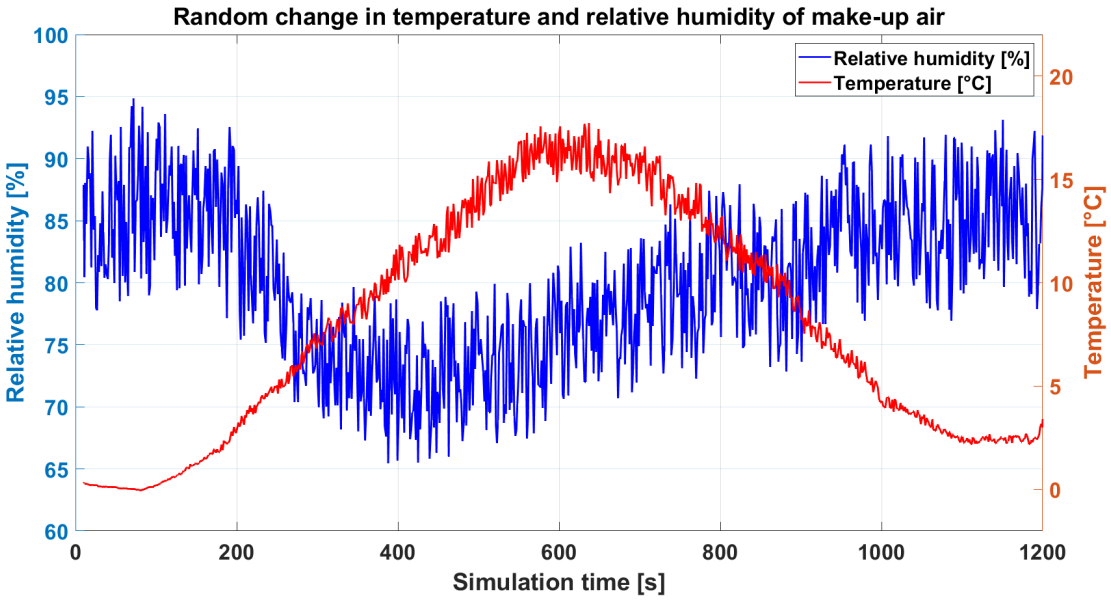

Figure 4.34: Random change in input temperature and relative humidity for make-up air

The purge rate of the airflow in the desiccant wheel will have a large impact on the air management system in terms of power demand and waste heat temperature. Changing the value used in the Baseline simulation from 8.17%, to 4% and 12%, will display the impact of a reduced and increased purge rate for Scenario 4 and 5. Scenario 4 is expected to have a reduced power demand, as less make-up air is required to maintain sufficient airflow to keep the moisture content of the dry room at 0.44 gr/lb. However, this comes with a trade-off in a reduced lifetime of the heat exchanger and increased maintenance. Similarly, the increased purge rate is expected to elevate these values.

Chapter 5

Further Use of Waste Heat

The Norwegian Minister of energy has made it mandatory for large scaled electricity powered industries that are under construction or upgrading, to analyze waste heat and its potential to be for further used [61]. Currently, it will not be required to act on the analysis, regardless if it is economically beneficial or not. However, to make this solution more attractive for the industries, reducing energy taxes for those who incorporate waste heat recovery is a potential solution. This will be an initiative for the green shift by reducing the energy losses and possibly using this otherwise lost energy instead of other energy sources. The cleanest energy is the one that does not needs to be produced.

5.1 Quality of Waste Heat

There are two main challenges for further use of waste heat: establishing demand and utilizing the low temperatures. The quality of the waste heat is a term used to cover the temperature, form and amount to determine the potential for further use. These factors are examined to get a better understanding of the potential application in this case.

Temperature
The temperature of the waste heat will be within the range of 36.13-47.73°C, depending on the size of the heat exchanger. This temperature range is challenging to utilize for other purposes than direct use for heating and drying, as displayed in Table 2.2. Mature technologies such as ORC and Kalina Cycles requires higher temperatures for heat conversion to power production. As the name indicates, the waste heat is usually just released into the surroundings and lost. Establishing a local demand will be vital to make this a viable use due to the poor energy potential with this temperature. Industries will have a low willingness to pay for this energy, making it rarely utilized regardless of its abundance in different sectors [30].

Form
Waste heat is most commonly in one of two forms; exhaust gasses or wastewater. Due to the different properties of the two mediums shown in Table 2.3, water is the more preferred of the two. With a higher specific heat capacity and density, water requires less volume for the same energy amount compared with air. This makes it easier and cheaper to transport to other locations with a more concentrated medium and lower transmis-

sion losses in pipes/ducts. Low-grade exhaust gasses should have direct use without any conversion between source and demand. Placing the demand outside the factory wall will also be preferable, similarly to the reasons described in the temperature description.

Amount

The amount of waste heat available, assuming a constant purge rate of 8.17%, will depend on the mass flow rate. The variations of the mass flow, and consequently the waste heat flow, changes seasonally. Higher temperatures and humid air in the summer half result in an increase in mass flow rate as it brings more moisture into the system through the make-up air. In Fig.5.1 the relationship between the temperature and the mass flow of the waste heat is displayed. The heat exchanger cannot extract the same amount of heat with a high mass flow, leaving a higher temperature of waste heat. The combination of higher temperature and more mass gives the airflow in the summer half of the year the most potential energy.

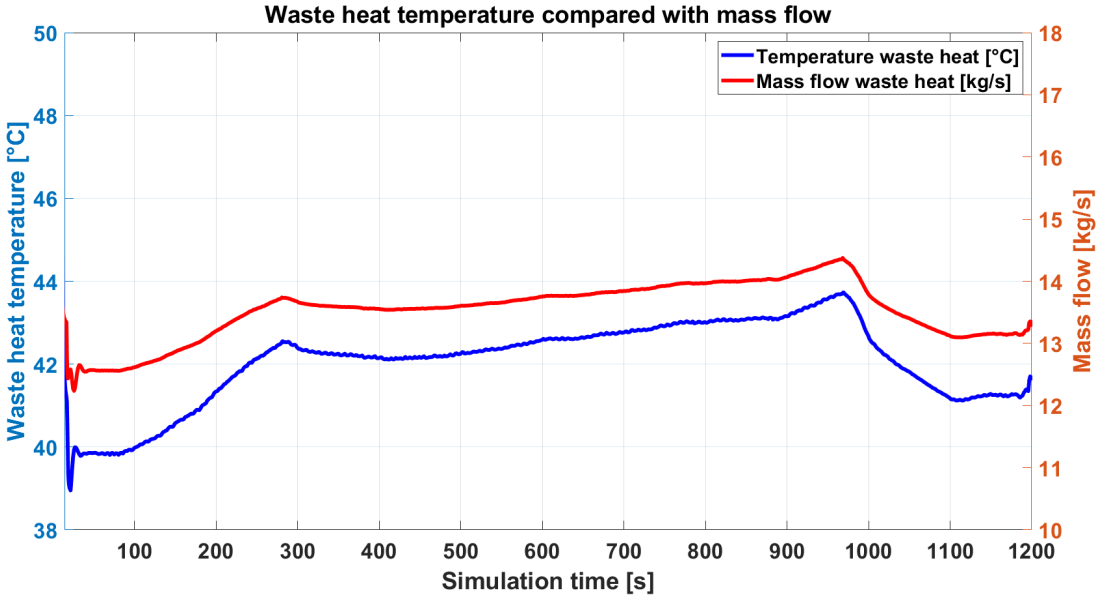

Figure 5.1: Temperature and mass flow of waste heat

The availability of the waste heat coincides with the amount, as it is assumed a constant operation of the dry room factory with 8760-hour operation each year. During the production of lithium-ion batteries, it is expected that the drying process is the bottleneck of the process. This could mean that there are some delays in the supply of battery cells for the factory. If the given factory shuts down at night, the moisture load from personnel would be removed, reducing the required mass flow through the room. This will result in a more uneven flow of waste heat, changing during the day. However, in this thesis, the operation in the dry room is assumed to be continuous and the values used are annual averages.

5.2 Potential Use Based on Quality

The objective is to achieve synergy by identifying another industry with a demand similar to the available supply. The waste heat is a secondary product from the air management system, so there will not be major altercations to change temperature or amount in improve the waste heat recovery system, as this will negatively impact the overall system. One of the largest challenges regarding waste heat recovery is the mismatch between supply and demand. Potential industries for the use of waste heat of the types produced by a dry room are listed below [30], based on the quality of the waste heat.

- Drying of wood chips
- Food production
- Heating

Of the three, drying of wood chips seems to have the largest potential for further use. According to the energy supply of waste heat, there is a potential to adapt the sizing of the drying process by using drying containers. The exhaust air can be used directly and without transporting, keeping the production right outside the factory walls. The system will not need any backup, as the drying of wood chips can be deemed a nonessential process.

For food production, greenhouses or land-based fish farms are the types best suited for waste heat [30]. However, both of them traditionally uses waste heat in liquid form as wastewater. By using an air-water heat exchanger, it is possible to convert the mediums. This requires more investment costs and transmission losses during the process, making it less desirable than industries using the heat directly and without any transmission. Especially as the energy content is very low, other solutions should be looked at.

For heating purposes, the most common temperatures of this range are defrosting/melting or keeping storage units frost-free. This is possible to do directly with exhaust gasses as a heat medium, but this application is highly seasonal. With the largest energy supply in the summer half for the waste heat, this will be a mismatch between demand and supply.

5.3 Drying of Wood Chips

From the Norwegian project report "Frå kratt til kroner" [4] the relationship between elevated air temperatures in drying of biomass and drying time has been investigated. By incorporating a solar collector into the cold air drying process, there was an apparent reduction of drying time due to higher moisture reduction, as displayed in Fig. E.1. With the availability of waste heat, it is possible to emulate the same optimal drying conditions throughout the year, not only on hot summer days. By expanding the period for the drying, the amount of dry biomass will increase. Reducing the moisture content of wood chips from its raw form of 50% down to 20%, the calorific value increases from 504 to 697 kWh/m^3. With a lower moisture content, the efficiency of the combustion process increases from 62% to 77%, which is taken into account for the calorific values.

There will be reduced emission due to a cleaner combustion, and the lifetime of the plant increases. Removing more moisture than down to 20% is not purposeful as the biomass would start to adsorb moisture from the ambient air.
The use of drying containers, as displayed in Fig. 5.2, makes it is possible to locate the drying right outside the factory walls. This will reduce the investment cost and transmission losses from large ducts transporting the waste heat.

Figure 5.2: Container drying of wood chips [62]

In the calculations from the project report, the temperature increase is based on what is vaguely defined as a "normal summer day" as a reference point, without mentioning any specific temperature. Therefore, the high average temperature of the three summer months, June, July and August, from Fig. 4.2 is calculated to be 18.2°C and used further. Fig E.1 shows the relationship between temperature increase and drying rate. The drying rate is the factor the drying time reduces, and correlates to the moisture removal rate given with the unit of measurement, g/m^3.
Combining the waste heat airflow with ambient air provides a larger mass flow, with a constant temperature. Newton-Raphson's method was used to solve the ratio, using annual average values to calculate the mass flow.

$$T_w\, x \,+\, T_a\,(\,1 \,-\, x\,) \,=\, T$$

$$42.64\, x \,+\, 7.78\,(\,1 \,-\, x\,) \,=\, 26.2 \Longrightarrow x \,=\, 0.528$$

This makes the waste heat airflow 52.8% of the total airflow, and ambient air the remaining 47.2%. This makes it possible to calculate the mass flow of the total airflow.

$$\dot{M} = \dot{m} + \dot{m} * \frac{(1 - x)}{x} = 13.53\,kg/s + 13.53\,kg/s * \frac{0.472}{0.528} = 25.63\,kg/s$$

Where:
T = Set temperature for drying, °C
T_a = Ambient temperature, °C
T_w = Waste heat temperature, °C
$\dot{M}$ = Mass flow air for drying, kg/s
$\dot{m}$ = Mass flow waste heat, kg/s

With an expected air density of 1.225 kg/m^3, the volumetric airflow is:

$$\frac{25.63\,kg/s}{1.225\,kg/m^3} = 20.92\,m^3/s$$

Wood chips with a moisture content of 50%, based on pine, has to remove 330 kg/m^3 water to reach 20% [4]. With a moisture removal of 2.9 g/m^3, the moisture removal is:

$$2.9\,g/m^3 * 20.92\,m^3/s = 60.66\,g/s$$

As 330 kg moisture corresponds to 1 m^3 wood chips at 20% moisture content, the rate of drying is:

$$\frac{60.66\,g/s}{330,000\,g/m^3} = 1.84 * 10^{-4}\,m^3/s = 0.662\,m^3/h = 5,797\,m^3/year$$

With the increased calorific value, the annual increase in energy potential is:

$$5,795 m^3/year\,(697\,kWh/m^3 - 504\,kWh/m^3) = 1,118,435\,kWh/year$$

Using the same approach to calculate for different temperatures, based on moisture removal rate from temperature increases of 2, 5, and 8°C, with a corresponding drying rate of 1.5, 2.2 and 2.9. The values are from Fig. E.1.

Chapter 6

Results

This chapter contains the result of the simulation of the air management system, which includes air quality, sizing of the heat exchanger, power demand for temperature control and the sensitivity analysis for different scenarios. Finally, the best solution for further use of the waste heat is presented, based on the quality and local demand at the factory site.

6.1 Air Quality

The outlet moisture content and temperature of the dry room air are presented in Figs. 6.1 and 6.2. This moisture content of 0.44 gr/lb is equivalent to a dew point temperature of -42°C and is kept constant as the main priority of the air management system. Air mass flow will be regulated to maintain a constant moisture content, and a heater/cooler used to keep the temperature between 22 and 25°C. With these two parameters within their respective limits, the air quality of the dry room is at a sufficient level.

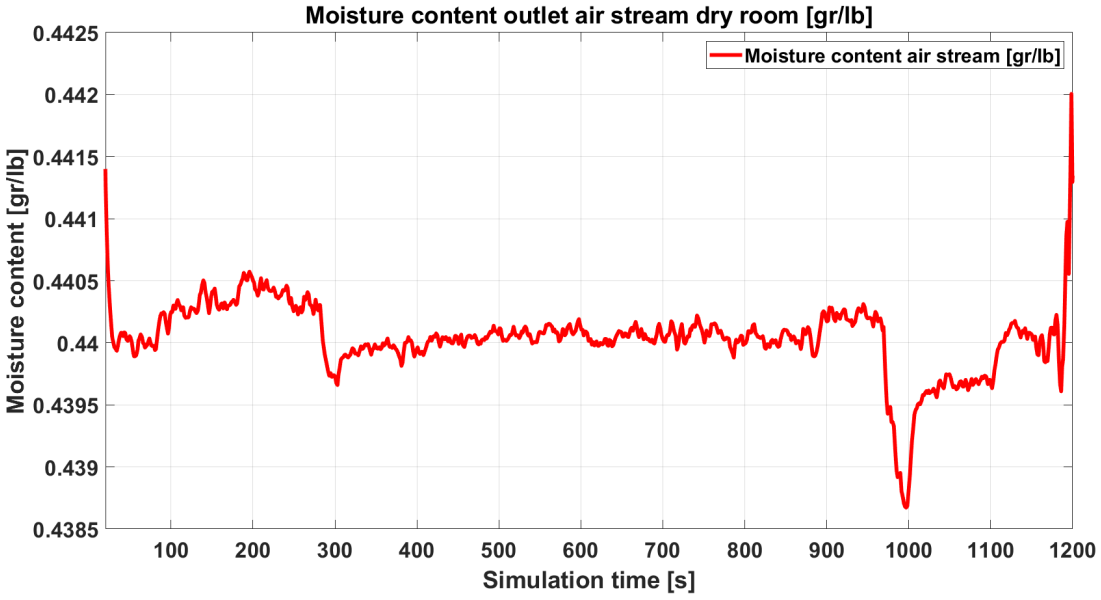

Figure 6.1: Moisture content of the outlet air from the dry room

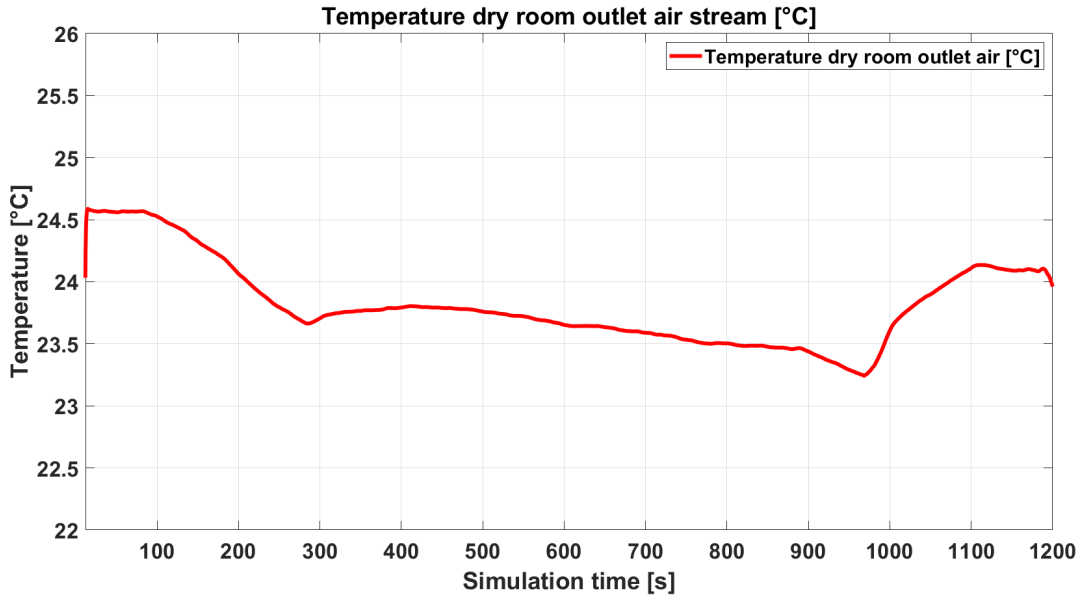

Figure 6.2: Temperature of the outlet air from the dry room

6.2 Sizing the Heat Exchanger

The size of the heat exchanger used in the regeneration heater loop depends on the overall cost. The overall cost is calculated by combining investment and O&M cost of the heat exchanger, with the cost of power production from the regeneration heater. More of the energy is recovered and reused with an increased heat transfer area, represented by the UA-value, leading to a decreased waste heat temperature.

The power measurements are for the regeneration heater, which heats the airflow to 146°C regardless of the waste heat temperature, using electricity as fuel. With a larger heat transfer area, there are higher expenditures for the heat exchanger, but the power demand from the regeneration heater decreases. Table 6.1 and Fig. 6.3 presents the results for the sizing of the heat exchanger, with UA-values, waste heat temperatures power demand and cost.

Table 6.1: Simulation results for different heat transfer areas of the heat exchanger

UA-value [kW/K]	Waste heat temperature [°C]	Power [kW]	Cost [mill NOK]
0	139.41	1758.1	43.74
10	87.64	1054.3	27.63
20	66.62	767.2	21.77
30	55.04	610.3	19.27
40	47.73	511.4	18.21
50	42.64	442.4	17.77
60	38.97	392.6	17.94
70	36.13	354.1	18.26
80	33.92	324.2	18.92
90	32.13	299.9	19.72
100	30.60	279.2	20.48
125	27.86	242.1	23.01
150	25.94	216.1	25.81
175	24.49	196.5	28.64
200	23.41	181.8	31.72

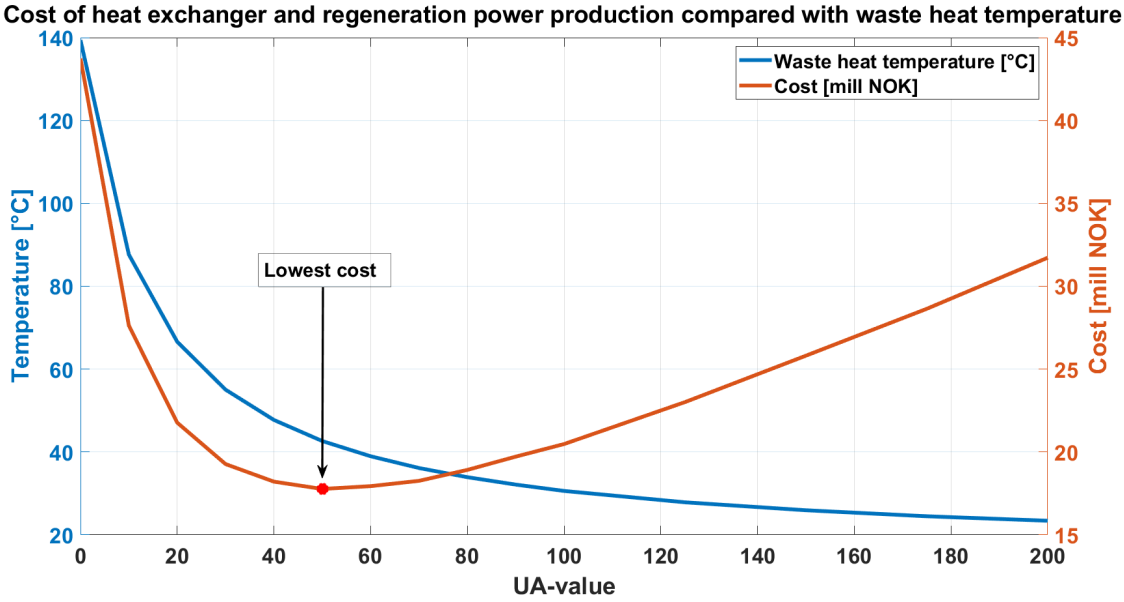

Figure 6.3: Comparison between lifetime cost of heat exchanger and energy cost, with resulting waste heat temperature

The optimal UA-value, which gives the lower overall cost, is 50 kW/K for the heat exchanger. The conversion between UA-values and heat transfer areas is presented in Table C.1, where a UA-value of 50 translates to a heat transfer area of 2,500 m^2. By using this size, the corresponding waste heat temperature is 42.64°C as an annual average. The actual cost of the heat exchanger, investment and operation, may deviate from the results presented as they are based on average prices.

With seasonal fluctuations, there are some variations in the waste heat temperature during the year, and the changes can be viewed in Fig. 6.4.

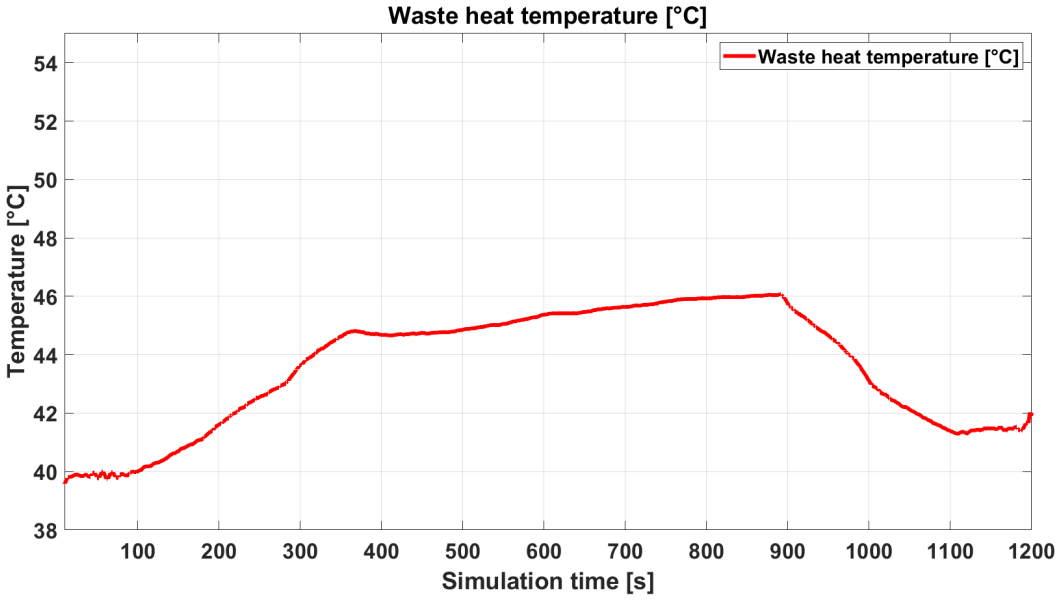

Figure 6.4: Annual fluctuation in waste heat temperature

The temperature will follow this trend, regardless of the heat exchanger size. The temperature rise is due to the increased mass flow in the summer half, making the heat transfer area of the heat exchanger less efficient. The UA-values of 50 will be used further in the following simulations and referred to as the Baseline simulation.

6.3 Power Demand

The overall power demand for temperature control of the air for one year is displayed in Fig. 6.5, where each 100-second interval represents one month, starting in January.

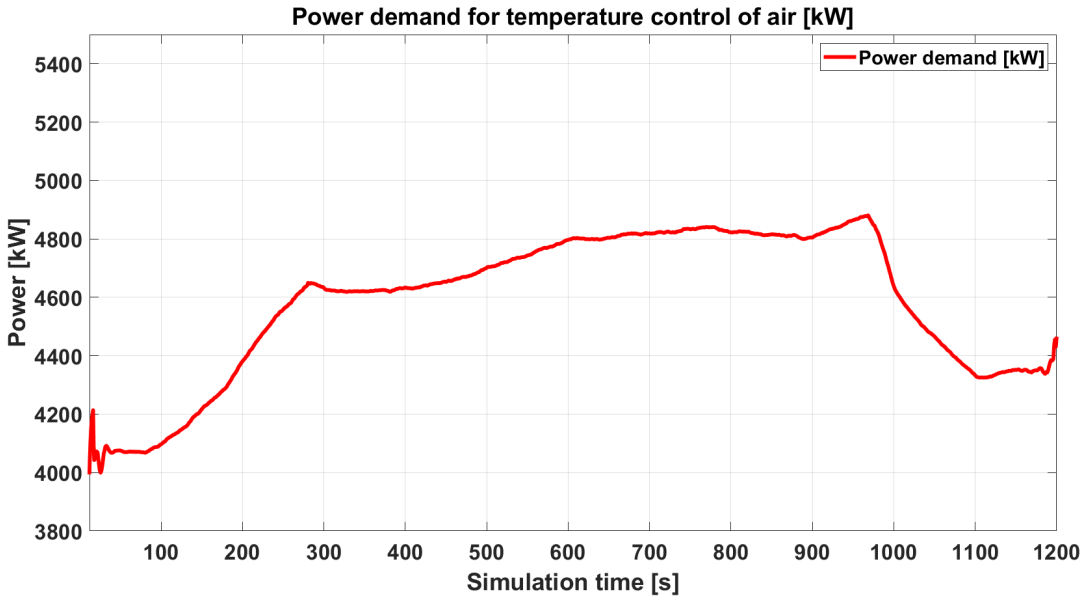

Figure 6.5: Power demand for temperature controlling air

The power curve corresponds to the mass flow of the air stream, displayed in Fig. 6.6, which again follows the seasonal trend. From April to October, the power demand is at its highest due to the increased moisture capacity of the elevated ambient temperatures. With more moisture in circulating the system, air mass flow is increased to keep the moisture content of the room at 0.44 gr/lb and more energy is required for temperature control and dehumidification. The average power demand during the year for the Baseline simulation results is 4,560 kW

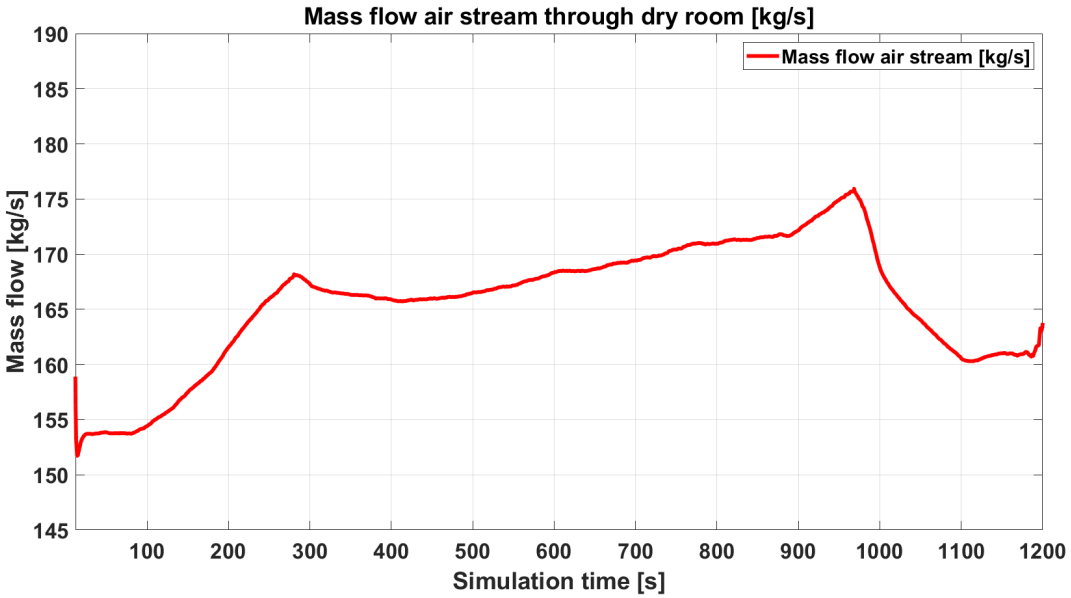

Figure 6.6: Mass flow air stream

6.4 Sensitivity Analysis

The sensitivity analysis are conducted using different parameters for input values, temperature and relative humidity, and changing purge rates to examine the impact on the system. Scenario 1 and Scenario 2 shows increased and decreased input temperature and relative humidity, changing the annual averages of the Baseline with +/-5%. Scenario 3 shows the results for random spikes in temperature and relative humidity within a +/-10% range from the mean Baseline values. The annual averages are the same as for Baseline for this Scenario 3, but with deviations from the mean values.

Scenario 4 and 5 shows the results of changing the purge rate from Baseline of 8.17% to 4% and 12%, respectively. In these scenarios, the ambient conditions are at Baseline values. These results of the sensitivity analysis are presented in Table 6.2.

Table 6.2: Sensitivity analysis results

	Power [kW]	Waste heat temperature [°C]	Mass flow [kg/s]
Baseline	4,561	42.64	165.6
Scenario 1	4,667	43.24	168.6
Scenario 2	4,216	40.72	156.5
Scenario 3	4,105	40.09	153.1
Scenario 4	3,596	27.21	145.7
Scenario 5	6,044	57.47	200.3

Scenario 1 and 2 showed expected results, where the power demand, waste heat temperature, and mass flow followed the rise and decrease of the input values. It should be noted that the 5% decrease showed a larger impact in terms of percentage change from Baseline than the 5% increase. Scenario 3 showed an even more favourable case than the Baseline values. Even if the average values were the same, the power demand, waste heat temperature and mass flow values got lower than the Baseline.

The changing of purge rates showed the impact it has on the system. As this value is proportional to the make-up air amount, the power demand and mass flow largely follow the purge rate, given that there will be more air that requires temperature control and dehumidification. With a higher amount of air, the current heat transfer area of the heat exchanger cannot efficiently adsorb the heat, and larger amounts of energy are lost as waste heat. The reverse happens when the mass flow is reduced with a lower purge rate. Sizing of the heat exchanger will therefor also depend on the purge rate used in the desiccant wheel, not only ambient conditions and moisture loads.

6.5 Drying of Wood Chips

Drying container placed right outside the factory walls will dry wood chips from a moisture content of 50% to 20%. Any drying below this point will be redundant, as the biomass would start to adsorb moisture from the surroundings to stabilise at 20% moisture content. Reduced moisture content ensures a better combustion process, as the efficiency increases from 62% to 77%, and reduction in contaminants from a cleaner combustion. The overall calorific value changes from 504 kWh/m^3 to 697 kWh/m^3 as a result.

Combining the waste heat and ambient air to keep a constant temperature, makes it possible to dry the wood chips throughout the year, and not only when in warm weather. Table 6.3 shows the results of the amount of dried wood chips and the increased energy content by reducing the moisture content from 50% to 20% on an annual basis for different temperatures.

Table 6.3: Drying of wood chips from 50% to 20% at different temperatures

Temperatures [°C]	Amount [m^3/year]	Energy increase [kWh/year]
18.2	3,530	681,290
20.2	4,447	858,271
23.2	5,254	1,014,022
26.2	5,797	1,118,821

Using a higher temperature will significantly reduce the wood chips' drying time due to a higher moisture removal rate. A higher temperature will result in a lower air mass flow as the ratio of waste heat and ambient air. With a constant temperature of 26.2°C, it is expected to dry 5,797m^3 of wood chips, increasing the energy potential with 1,118,821 kWh. These calculations take into account the increased calorific value and expected higher efficiency of the combustion process.
The drying process will be unevenly distributed during the year. Elevated ambient air temperatures at the time of most energy available as waste heat causes the air flow in the summer to be higher than in the winter. The results presented are therefore a yearly production.

The desiccant wheel for the dehumidification process can use both thermal and electrical energy for regeneration heating. With the expected calorific value of the wood chips with 20% moisture of 697 kWh, the annual energy is 4,040,509 kWh for the 5,797 m^3 of wood chips, or an average power production of 461.2 kW. Comparing this to the average power demand of the regeneration heat at 442.4 kW, using wood chips for this heating could cover the power demand. Selecting a combustion process using wood chips for the regeneration heater instead of an electrical heater is possible, and would utilize the waste heat available from the factory.

Chapter 7

Discussion

7.1 Air Quality

Determining the definition of the air quality in the dry room is based on information from various dry room producers for lithium-ion battery production. They have stated that the two most important factors are temperature and moisture content. By keeping the temperature of the exiting air between 22 and 25°C and the moisture content stable at 0.44 gr/lb, the quality of the air is deemed sufficient for dry room conditions for lithium-ion battery production. The used of dew point as a moisture content measurement is common for dry room applications, and 0.44 gr/lb translates to either -42°C or 100 PPMV.

If these values are surpassed it would negatively affect the battery cells. Moisture within the sealed cells could potentially start chemical reactions with the battery material. This would diminish the quality, lifetime and performance of the cell, and in worst case cause a short circuit leading to a fire or explosion.

7.2 Sizing the Heat Exchanger

The temperature of the waste heat will depend on the sizing of the heat exchanger. A larger heat transfer area will be able to extract more of the energy before releasing it as waste heat and consequently reduce the power demand from the regeneration heater. However, a larger heat exchanger came with more costs for investment and use. The determination of the optimal solution for this thesis is based on the overall prices from the regeneration heater system, which includes all costs involved with the heat exchanger and the power cost for the heater. Incorporating a heat exchanger will definitely reduce the overall cost and efficiency of the system, but the size will depend on the actual prices for the given factory. As these prices are approximations, the actual result for the given factory may deviate some from these result.

The results of the simulation in this thesis shows that a UA-values of 50 kW/K gives the lowest cost. However, in the range 40-70 kW/K there are small changes in the overall cost, but the temperature of the waste heat changes from 36.13°C to 47.73°C. The size of the heat exchanger may also be relevant for the factory, as the heat transfer area is 2,000 m^2 for a UA-value of 40, and 3,500 m^2 a UA-value of 70. This relationship is displayed in in Table C.1. The given factory may have site specific differences, making it more pre-

disposed for one or the other ends of the spectre depending on the most desirable waste heat temperature, area of heat exchanger and actual prices.

7.3 Power Demand

The power demand calculated for the dry room covers the temperature control of the air management system. Other contributing sources, such as other equipment and fans, have not been taken into consideration in this thesis. During the year, the power demand will experience seasonal fluctuations. Due to elevated temperatures with higher moisture content from April to October, the system will have to operate at a higher capacity. More moisture in the make-up air requires a higher air mass flow, leading to more air that needs temperature control and dehumidification. The waste heat temperature will also follow this seasonal fluctuation, as the increased mass flow makes the heat exchanger unable to adsorb the heat at the same rate.

7.4 Sensitivity Analysis

By running a sensitivity analysis for potentially changing parameters, the durability and weaknesses of the system are exposed. Ambient conditions are constantly changing, although they keep a rather even annual average. Increasing and decreasing the temperature and relative humidity by 5% from Baseline, the results were as expected. The power demand, waste heat temperature and mass flow followed this change. However, the results changed unexpectedly by simulating with random peaks of +/-10%. With the same input average as the Baseline, the power demand changed favourably with a 10% decrease. This proves that the system is not only sufficient during varying conditions, but actually improves.

The final changed parameter is the purge rate for the desiccant wheel. Initially, this was set to be 8.17% and changed to 4% and 12% in the sensitivity analysis. As expected, the values followed accordingly as the make-up air is proportional to the purge rate. The trade-off to lower power demand and waste heat is the build-up of unwanted contaminates and a reduced lifetime of the heat exchanger. More moisture will also accumulate in the molecular sieve, resulting in a higher regeneration temperature for the desorption process. This will cause more stress to the desiccant, and potentially a reduced lifetime for it as-well. To what extent the rate of contaminant build-up compared to the purge rate is unknown.

The decision to set the Baseline value at 8.17% was based on the expected contamination level of a desiccant wheel using high regeneration temperatures (140-170°C). More research for the specific wheel used in this factory may change the purge rate/section size. This will further have a large impact on the overall power demand, as the sensitivity analysis has presented.

7.5 Drying of Wood Chips

The use of waste heat for drying wood chips is one of the multiple different applications considered and is meant to be a suggestion for potential use. Given the low temperature of the waste heat, it is hard to find a good use for it and is the main reason most of this type of energy is currently lost to the surroundings. The drying of wood chips usually uses a similar technique with cold air drying, using fans and the ambient air. Combining the ambient air with the waste heat and using containers for the drying process makes it possible to use the waste heat directly without any transportation. Wood chips can be used as fuel for the regeneration heater, creating a local demand for this solution. There are uncertainties associated with selecting this solution, as it is very dependant on the local interest and demand.

The use of wood chips for the regeneration heater looks to be the solution with the most potential. Altering between the electrical heating and the thermal combustion process could also be possible, taking advantage of fluctuating electricity prices.

Chapter 8

Conclusion

- The main priority in the air management system is to keep the air quality at dry room conditions. This is defined with a moisture content at 0.44 gr/lb and a temperature of 22-25°C. This was achieved by using a combined dehumidification system with a desiccant wheel using molecular sieve and mechanical dehumidifying coolers.
- The power demand is minimised by testing different temperatures for the temperature controlling units in the air management system, averaging 4,560 kW.
- Incorporating a heat exchanger in the regeneration loop for the purge airflow will reduce the overall cost and improve the efficiency of the system. By reusing the thermal energy in the waste heat, less power is required by the regeneration heater to reach the temperature of 146°C for desorption of moisture from the desiccant wheel. The optimal UA-value for the heat exchanger is 50 kW/K, but sizes in the 40-70 kW/K range will still have a competitive price, and the site specifications will be determining for the sizing.
- The waste heat temperature of the exhaust air will be 42.6°C as an annual average, with seasonal changes giving max and min values of 39.8 and 43.7°C. The air mass flow is on average 165.4 kg/s with minimal and maximal values of 153.8 and 175.9 kg/s. Again, it follows the seasonal pattern discovered where the highest values are in the summer, where higher temperatures of the make-up air contains a higher moisture content.
- By using different purge rates for the desiccant wheel, the power demand changed as the purge rate is proportional to the make-up air. Purge rates of 4% and 12% have been tested, where a higher purge rate increases the power demand and the lower reduced it compared to the Baseline purge rate of 8.17%. There is a trade-off with a lower purge rate, as it results in a reduced lifetime and more maintenance of the heat exchanger.
- Drying of biomass has been investigated as a possible use for the waste heat produced from the dry room. Increasing the temperature of the drying process from 18.2 to 26.2°C reduced the time required to dry wood chips. It is expected to dry 5,797 m^3/year of wood chips from 50% moisture content to 20% by using the waste heat for drying of wood chips from the dry room in combination with ambient air. As the drying containers investment and operation costs are currently unknown, it is still not confirmed if it will be profitable to invest in a system like this.

8.1 Further Work

Recovery and distribution of waste heat requires a small-scale setup. For factories, there are often multiple waste heat sources. By centralizing different heat streams into one, it is possible to decrease investment costs and transmission losses. In battery factories, another waste heat source is from the drying of the electrode materials, where moisture and solvents are evaporated. It would be interesting to look at the waste heat potential in this part of the production process and combine the different sources. Especially promising is the NMP solvent recovery. At this stage, it is assumed to be large amounts of waste heat, and by combining these sources, the quality of the waste heat would increase, making it more desirable to use.

Looking at other possible uses of waste heat than drying of biomass. Other possibilities were ruled out in this thesis, depending on the available industries, and their willingness to invest in other areas could make them more viable.

Bibliography

[1] Yangtao Liu et al. "Current and future lithium-ion battery manufacturing". In: *iScience* 24.4 (Apr. 2021), p. 102332. ISSN: 2589-0042. DOI: 10.1016/j.isci.2021.102332.

[2] Olje- Og energidepartementet. "Vil energieffektivisere ved å utnytte overskuddsvarme fra datasentre". In: *Regjeringen* (Feb. 2021). URL: https://www.regjeringen.no/no/aktuelt/vil-energieffektivisere-ved-a-utnytte-overskuddsvarme-fra-datasentre/id2835232.

[3] *Batterifabrikken i Mo i Rana*. [Online; accessed 8. May 2021]. Nov. 2020. URL: https://new.siemens.com/no/no/siemens-i-norge/nyheter/industri/batterifabrikken.html.

[4] Kåre Kristen Totlund and Ola Tjelle. *Frå kratt til kroner*. https://www.statsforvalteren.no/contentassets/39c48269ff8047f5b956387387b6bed9/fra-kratt-til-kroner-2005---2008-_prosjektrapport.pdf.

[5] Tsutomu Ohzuku and Ralph J. Brodd. "An overview of positive-electrode materials for advanced lithium-ion batteries". In: *J. Power Sources* 174.2 (Dec. 2007), pp. 449–456. ISSN: 0378-7753. DOI: 10.1016/j.jpowsour.2007.06.154.

[6] Yuanli Ding et al. "Automotive Li-Ion Batteries: Current Status and Future Perspectives". In: *Electrochem. Energ. Rev.* 2.1 (Mar. 2019), pp. 1–28. ISSN: 2520-8136. DOI: 10.1007/s41918-018-0022-z.

[7] Llc Keith Araujo- Epec. *Battery Comparison of Energy Density - Cylindrical and Prismatic Cells*. [Online; accessed 8. Dec. 2020]. Sept. 2020. URL: https://www.epectec.com/batteries/cell-comparison.html.

[8] Robert Schröder, Muhammed Aydemir, and Günther Seliger. "Comparatively Assessing different Shapes of Lithium-ion Battery Cells". In: *Procedia Manuf.* 8 (Jan. 2017), pp. 104–111. ISSN: 2351-9789. DOI: 10.1016/j.promfg.2017.02.013.

[9] Lesics. *Lithium-ion battery, How does it work?* [Online; accessed 24. May 2021]. Apr. 2019. URL: https://www.youtube.com/watch?v=VxMM4g2Sk8U.

[10] John B. Goodenough. "How we made the Li-ion rechargeable battery". In: *Nat. Electron.* 1.3 (Mar. 2018), p. 204. ISSN: 2520-1131. DOI: 10.1038/s41928-018-0048-6.

[11] Jiahui Liu. *Charge and Discharge Characterization of Lithium-ion Electrode Materials Through Coin Cell Testing*. https://kb.osu.edu/bitstream/handle/1811/68620/1/Thesis.pdf.

[12] *Electrochemical Potential | PVEducation*. [Online; accessed 3. Feb. 2021]. Feb. 2021. URL: https://www.pveducation.org/pvcdrom/battery-basics/electrochemical-potential.

[13] *BU-306: What is the Function of the Separator? – Battery University*. [Online; accessed 19. May 2021]. May 2021. URL: https://batteryuniversity.com/learn/article/bu_306_battery_separators.

[14] Christopher J. Orendorff. *The Role of Separators in Lithium-Ion Cell Safety*. https://www.electrochem.org/dl/interface/sum/sum12/sum12_p061_065.pdf.

[15] *Lithium-ion Batteries Information - Battery University*. [Online; accessed 26. Mar. 2021]. Mar. 2021. URL: https://batteryuniversity.com/learn/archive/understanding_lithium_ion.

[16] *How to Prolong Lithium-based Batteries - Battery University*. [Online; accessed 17. Sep. 2020]. July 2019. URL: https://batteryuniversity.com/learn/article/how_to_prolong_lithium_based_batteries.

[17] *Battery Power Online | Thermal Runaway: Understanding the Fundamentals to Ensure Safer Batteries*. [Online; accessed 26. Mar. 2021]. Sept. 2019. URL: https://www.batterypoweronline.com/news/thermal-runaway-understanding-the-fundamentals-to-ensure-safer-batteries.

[18] University of Sheffield Mark Winter and WebElements Ltd. *WebElements Periodic Table » Lithium » reactions of elements*. [Online; accessed 25. Feb. 2021]. Feb. 2021. URL: https://www.webelements.com/lithium/chemistry.html.

[19] *dry rooms lithium battery manufacturing | Bryair*. [Online; accessed 18. Jan. 2021]. July 2018. URL: https://www.bryair.com/fr/eu-fr/products-solutions/dry-rooms-lithium-battery-manufacturing.

[20] Hui Yang, Guorong V. Zhuang, and Philip N. Ross. "Thermal stability of LiPF6 salt and Li-ion battery electrolytes containing LiPF6". In: *J. Power Sources* 161.1 (Oct. 2006), pp. 573–579. ISSN: 0378-7753. DOI: 10.1016/j.jpowsour.2006.03.058.

[21] *The effects of ambient storage conditions on the structural and electrochemical properties of NMC-811 cathodes for Li-ion batteries | Elsevier Enhanced Reader*. [Online; accessed 5. May 2021]. May 2021. DOI: 10.1016/j.electacta.2020.137358.

[22] F. E. Nia. "Sustainable Air Handling by Evaporation and Adsorption". In: *undefined* (2011). URL: https://www.semanticscholar.org/paper/Sustainable-Air-Handling-by-Evaporation-and-Nia/54463f75441bf5a75c65da81adaf9e2ffe845c98#citing-papers.

[23] *Method of operation - DehuTech AB*. [Online; accessed 1. Feb. 2021]. Oct. 2016. URL: http://dehutech.com/method-of-operation.

[24] *Desiccant Chart Comparisons - SorbentSystems.com*. [Online; accessed 29. Jan. 2021]. July 2017. URL: https://www.sorbentsystems.com/desiccants_charts.html.

[25] Kntgroup. *About Molecular Sieve (with subtitles)*. [Online; accessed 19. May 2021]. Apr. 2011. URL: https://www.youtube.com/watch?v=g351-MEeAJU.

[26] Jasper van Kampen, Jurriaan Boon, and Martin van Sint Annaland. "Steam adsorption on molecular sieve 3A for sorption enhanced reaction processes". In: *Adsorption* (Nov. 2020), pp. 1–13. ISSN: 1572-8757. DOI: 10.1007/s10450-020-00283-8.

[27] Feng Huang et al. "Heat recovery potentials and technologies in industrial zones". In: *J. Energy Inst.* 90.6 (Dec. 2017), pp. 951–961. ISSN: 1743-9671. DOI: 10.1016/j.joei.2016.07.012.

[28] Hussam Jouhara et al. “Waste heat recovery technologies and applications”. In: *Thermal Science and Engineering Progress* 6 (June 2018), pp. 268–289. ISSN: 2451-9049. DOI: 10.1016/j.tsep.2018.04.017.

[29] Gløsen Breivik. *Mulighet for å utnytte lavtemperatur spillvarme fra prosessindustrien i Grenland*. https://www.sintef.no/globalassets/sintef-industri/prosjekter/gronne-sommerjobber/2019_08_30_muligheter-for-a-utnytte-lavtemperatur-spillvarme-fra-prosessindustrien-i-grenland.pdf.

[30] Linda Pedersen Haugerud. *Smart bruk av spillvarme og grønn næringsutvikling*. https://www.ringerike.kommune.no/contentassets/ae3218f9c8974c298a50098b8c8b3a6d/smart-bruk-av-spillvarme-og-gronn-naringsutvikling_konseptutredning-ringerike_endelig-sluttrapport.pdf.

[31] *How do heat exchangers work?* [Online; accessed 8. Apr. 2021]. Apr. 2021. URL: https://www.explainthatstuff.com/how-heat-exchangers-work.html.

[32] *Overall Heat Transfer Coefficient*. [Online; accessed 5. Apr. 2021]. Mar. 2021. URL: https://www.engineeringtoolbox.com/overall-heat-transfer-coefficient-d_434.html.

[33] *Thermal Conductivity of some selected Materials and Gases*. [Online; accessed 29. Apr. 2021]. Apr. 2021. URL: https://www.engineeringtoolbox.com/thermal-conductivity-d_429.html.

[34] *Mollier Diagram*. [Online; accessed 16. Feb. 2021]. Feb. 2021. URL: https://www.engineeringtoolbox.com/psychrometric-chart-mollier-d_27.html.

[35] Shabbir Ahmed, Paul A. Nelson, and Dennis W. Dees. “Study of a dry room in a battery manufacturing plant using a process model”. In: *J. Power Sources* 326 (Sept. 2016), pp. 490–497. ISSN: 0378-7753. DOI: 10.1016/j.jpowsour.2016.06.107.

[36] Morten Klaussen, Zhilwan Manbari, and Svein Sundsdal. “Vil bygge batterifabrikk til over fem milliarder kroner”. In: *NRK* (May 2020). URL: https://www.nrk.no/sorlandet/vil-bygge-batterifabrikk-til-over-fem-milliarder-kroner-1.15023860.

[37] *A New 32GWh Gigafactory Will Build Sustainable Batteries In Norway*. [Online; accessed 17. Feb. 2021]. May 2020. URL: https://www.morrowbatteries.com/post/a-new-32gwh-gigafactory-will-build-sustainable-batteries-in-norway.

[38] Camilla Cole. *Morrow Batteries - Eyde energipark - Arendal kommune*. [Online; accessed 17. Feb. 2021]. Feb. 2021. URL: https://www.arendal.kommune.no/politikk-og-organisasjon/prosjekter-og-utvikling/batterifabrikk.

[39] *Google Maps*. [Online; accessed 20. May 2021]. May 2021. URL: https://www.google.co.uk/maps/place/Morrow+Batteries/@59.9613844,4.8918625,5.5z/data=!4m12!1m6!3m5!1s0x464795dab9cdc6c3:0x9f3db4040fc6c501!2sMorrow+Batteries!8m2!3d58.4998729!4d8.8020703!3m4!1s0x464795dab9cdc6c3:0x9f3db4040fc6c501!8m2!3d58.4998729!4d8.8020703?hl=en.

[40] *Morrow Batteries velger Arendal for batterifabrikken | Agder Energi*. [Online; accessed 17. Feb. 2021]. Feb. 2021. URL: https://kommunikasjon.ntb.no/pressemelding/morrow-batteries-velger-arendal-for-batterifabrikken?publisherId=16388593&releaseId=17898404.

[41] Yu Media Group d.o.o. *Arendal, Norway - Detailed climate information and monthly weather forecast | Weather Atlas*. [Online; accessed 9. Apr. 2021]. Apr. 2021. URL: https://www.weather-atlas.com/en/norway/arendal-climate#temperature.

[42] *Harris Environmental - The Dry Room System*. [Online; accessed 18. Jan. 2021]. June 2015. URL: http://www.harrisenv.com/dry_room_system.htm#specification.

[43] Dr. Rudolf Simon. *Qualitats- und Kostenoptimierung in Lithium-Ionen-Batteriefabriken*. Accessed: 5-1-2021.

[44] Heiner Heimes et al. *LITHIUM-ION BATTERY CELL PRODUCTION PROCESS*. Feb. 2019. ISBN: 978-3-947920-03-7.

[45] Zhao Jiang et al. "Research on vacuum drying process and internal heat conduction of Li-ion battery core". In: *Theor. Appl. Mech. Lett.* 9.2 (Mar. 2019), pp. 120–129. ISSN: 2095-0349. DOI: 10.1016/j.taml.2019.02.008.

[46] *Energy Storage | Electrode Manufacturing - Dürr Megtec*. [Online; accessed 16. Apr. 2021]. July 2020. URL: https://www.durr-megtec.com/en/products/energy-storage.

[47] Paul A. Nelson et al. "Modeling the Performance and Cost of Lithium-Ion Batteries for Electric-Drive Vehicles, Third Edition". In: (Mar. 2019). DOI: 10.2172/1503280. URL: https://www.osti.gov/biblio/1503280.

[48] Ali Alahmer, Sameh Alsaqoor, and Gabriel Borowski. "Effect of parameters on moisture removal capacity in the desiccant cooling systems". In: *Case Stud. Therm. Eng.* 13 (Mar. 2019), p. 100364. ISSN: 2214-157X. DOI: 10.1016/j.csite.2018.11.015.

[49] Amarjeet Kumar Prasad and Ravi Pratap. "Inclusion of Purge Sector in Rotary Desiccant Wheel: A Review". In: *International Journal of Engineering Research & Technology* 7.4 (Apr. 2018). ISSN: 2278-0181. URL: https://www.ijert.org/inclusion-of-purge-sector-in-rotary-desiccant-wheel-a-review.

[50] S. Slayzak and J. P. Ryan. "Desiccant Dehumidification Wheel Test Guide". In: *undefined* (2001). URL: https://www.semanticscholar.org/paper/Desiccant-Dehumidification-Wheel-Test-Guide-Slayzak-Ryan/06bf208dfb2ac9a03915afeddf4756a08bcf44b3.

[51] *Energy Recovery Wheel Purge | Semco HVAC*. [Online; accessed 5. Apr. 2021]. Apr. 2021. URL: https://www.semcohvac.com/applications/purge.

[52] *Harris Environmental - Korea Paper*. [Online; accessed 28. Jan. 2021]. June 2015. URL: http://www.harrisenv.com/korea_paper.htm.

[53] *Required Air to Remove Moisture*. [Online; accessed 5. Feb. 2021]. Jan. 2021. URL: https://www.engineeringtoolbox.com/moisture-remove-room-air-flow-d_1636.html.

[54] *Water Vapor in Air*. [Online; accessed 3. Feb. 2021]. Jan. 2021. URL: https://www.engineeringtoolbox.com/water-vapor-air-d_854.html.

[55] *NovelAire*. [Online; accessed 22. May 2021]. May 2021. URL: https://novtools.novelaire.com/DWWebApp.aspx.

[56] K.K. Thakur Surendra Vishvakarma Sanjay Kumbhare. "A REVIEW ON HEAT TRANSFER THROUGH HELICAL COIL HEAT EXCHANGERS". In: *INTERNATIONAL JOURNAL OF ENGINEERING SCIENCES RESEARCH TECHNOLOGY* (Aug. 2016). DOI: 10.5281/zenodo.60105.

[57] Marko Jarić et al. “Total costs of shell and tube heat exchangers with concentric helical tube coils”. In: *Thermal Science* 23.00 (Jan. 2019), p. 64. DOI: 10.2298/TSCI180727064J.

[58] Sabyasachi Mukherjee and P. Sivaniranjan. “DESIGN OF A TEMPERATURE CONTROL SYSTEM USING MATLAB FOR MILK PROCESS PLANT”. In: *International Journal of Multidisciplinary Research and Modern Education (IJMRME)* 2 (May 2016), p. 399. URL: https://www.researchgate.net/publication/320414667_DESIGN_OF_A_TEMPERATURE_CONTROL_SYSTEM_USING_MATLAB_FOR_MILK_PROCESS_PLANT.

[59] *Valutakurser*. [Online; accessed 20. Apr. 2021]. Apr. 2021. URL: https://www.norges-bank.no/tema/Statistikk/Valutakurser/?tab=currency&id=EUR.

[60] *2021-02-15*. [Online; accessed 20. Apr. 2021]. Apr. 2021. URL: https://www.ssb.no/elkraftpris.

[61] *Norway: "New requirements for waste heat from data centers"*. [Online; accessed 3. Apr. 2021]. Apr. 2021. URL: https://www.datacenter-forum.com/datacenter-forum/norway-new-requirements-for-waste-heat-from-data-centers.

[62] *Drying Stations | Woodchip Drying Containers | Stronga Drying Systems*. [Online; accessed 12. May 2021]. May 2021. URL: https://stronga.com/en/products/drying-stations.

[63] *Moisture conversion table*. https://www.asge-online.com/pdf/ASGEpg185.pdf.

Appendix A

Simulink Model

The actual Simulink system is displayed in Fig. A.1.

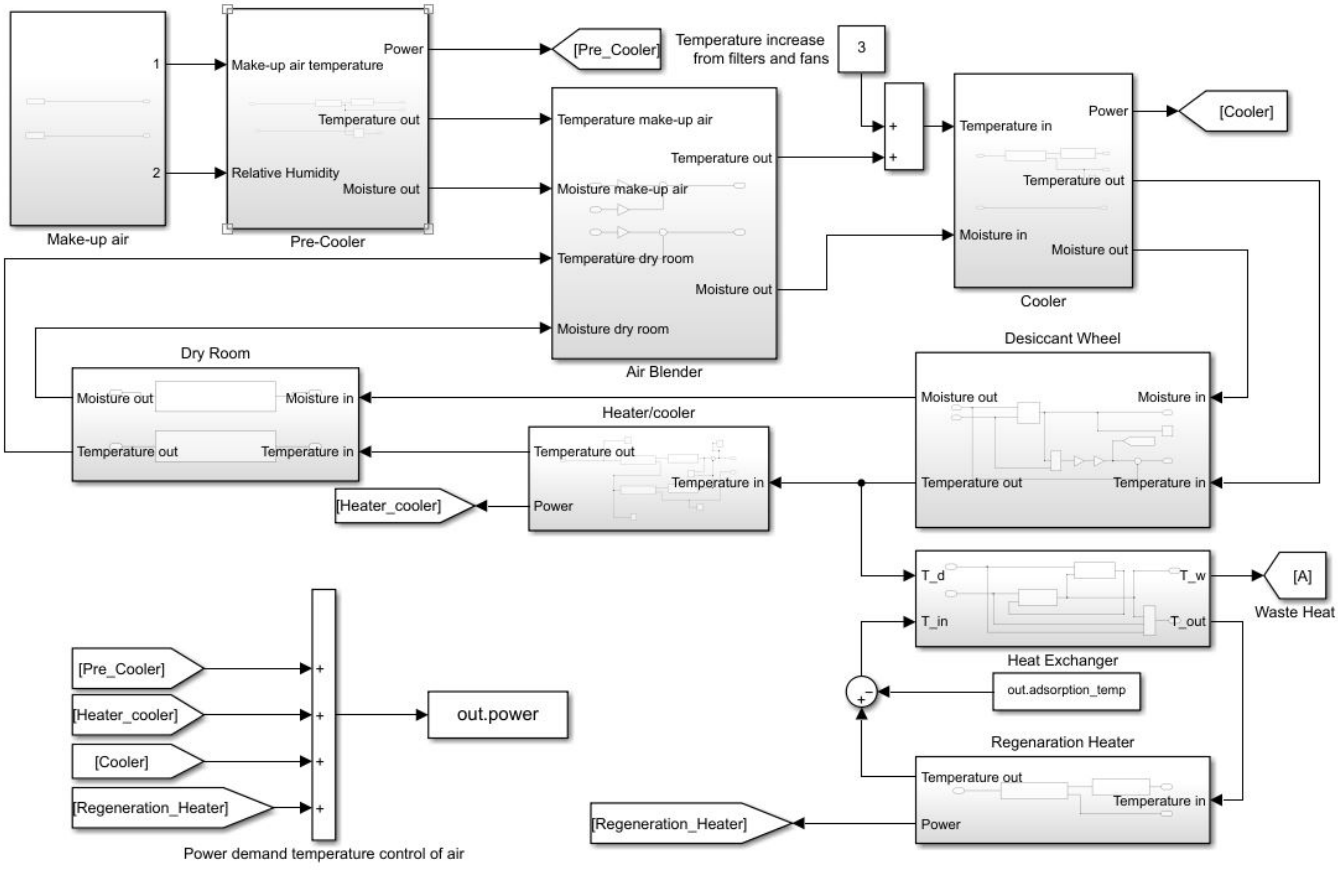

Figure A.1: Simulink system of air management system of the dry room

Appendix B

Moisture Conversion Table

Table B.1: Moisture conversion table [63]

Dew Point [°C]	PPMV	Relative Humidity [%] at 21.1 °C
-90	0.0921	0.00037
-86	0.184	0.00075
-82	0.382	0.00155
-78	0.737	0.00300
-74	1.38	0.00559
-70	2.55	0.0104
-66	4.59	0.0187
-62	8.08	0.0328
-58	13.9	0.0565
-54	23.4	0.0948
-50	38.8	0.157
-46	63.3	0.257
-44	80	0.325
-42	101	0.410
-40	127	0.516
-38	159	0.644
-36	198	0.804
-34	246	1.00
-32	305	1.24
-30	376	1.52
-28	462	1.88
-26	566	2.30
-24	692	2.81
-22	842	3.41
-20	1020	4.13
-18	1240	5.00
-14	1790	7.25
-10	2570	10.4
-6	3640	14.7
-2	5100	20.7
2	6970	28.2
4	8030	32.5
8	10590	42.9
12	13840	56.1
16	17930	72.6
20	23080	93.5

Appendix C

UA-values and Heat Transfer Area

Table C.1: Relationship between UA-value and heat transfer area

UA-value [kW/K]	Heat transfer area [m^2]
0	0
10	500
20	1,000
30	1,500
40	2,000
50	2,500
60	3,000
70	3,500
80	4,000
90	4,500
100	5,000
125	6,250
150	7,500
175	8,750
200	10,000

Appendix D

Conversion Parameters from Matlab Script

Parameter	Value	Description	Unit
c	1.0054	Specific heat capacity air	[kJ/kg K]
rho_g	1.225	Density air	[kg/m^3]
Purge_rate	0.0817	Purge rate airflow	[%]
Reuse_rate	0.9183	Reuse rate airflow	[%]
g_gr	0.0648	Grams per grain moisture	[-]
gr_g	1.5432	Grains moisture per gram	[-]
kg_lb	0.4536	Kg per lb	[-]
lb_kg	2.2046	Lb per kg	[-]
q_st	4186	Adsorption heat moisture using molecular sieve	[kJ/kg]

Appendix E

Drying Time for Wood Chips

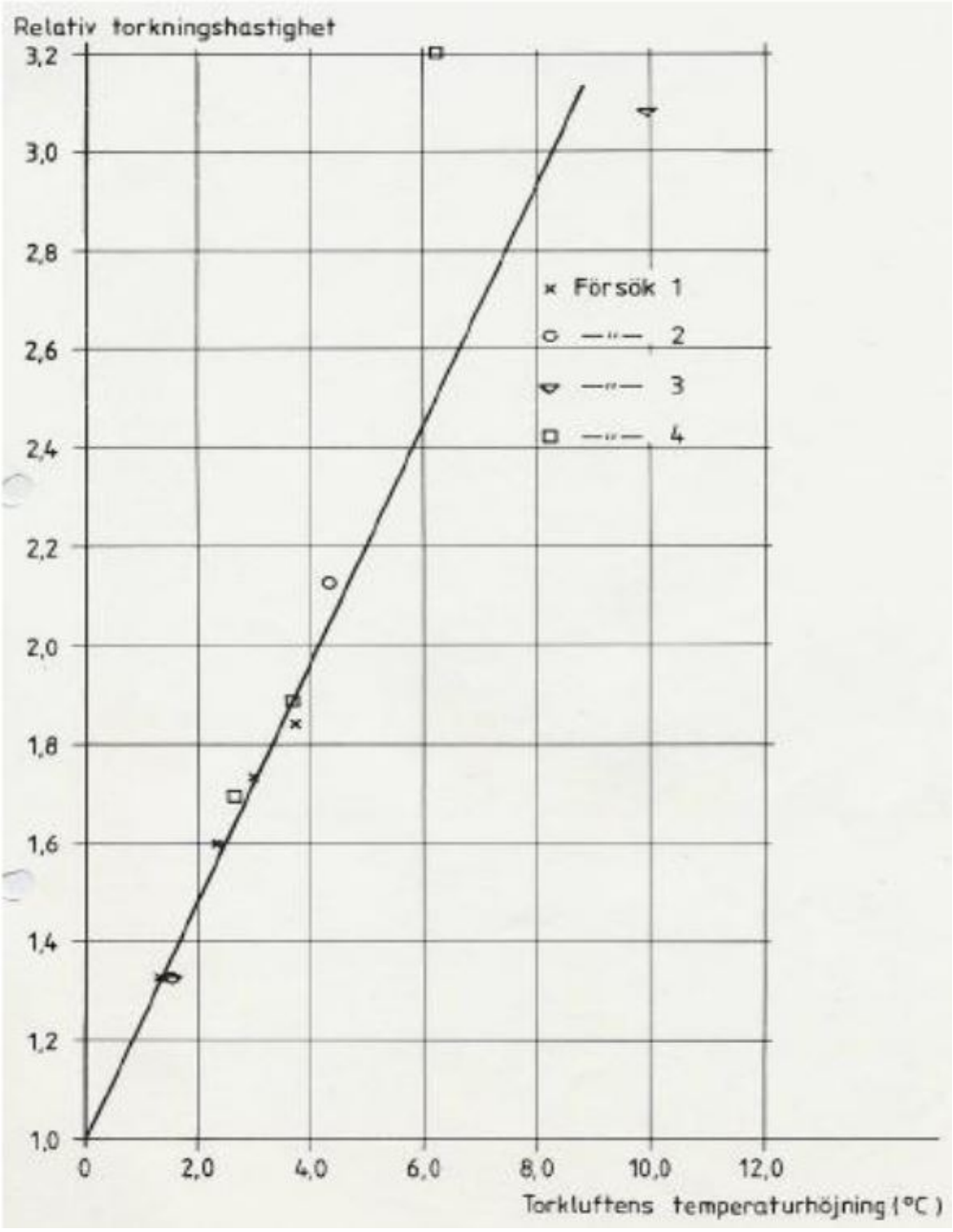

Figure E.1: Drying time reduction depending on temperature increase in air [4]